Understanding Microwave Surface-Wave Sustained Plasmas at Intermediate Pressure by 2D Modeling and Experiments

Violeta Georgieva,* Antonin Berthelot, Tiago Silva, Stanimir Kolev, Wouter Graef, Nikolay Britun, Guoxing Chen, Joost van der Mullen, Thomas Godfroid, Diana Mihailova, Jan van Dijk, Rony Snyders, Annemie Bogaerts, Marie-Paule Delplancke-Ogletree

An Ar plasma sustained by a surfaguide wave launcher is investigated at intermediate pressure (200–2667 Pa). Two 2D self-consistent models (quasi-neutral and plasma bulk-sheath) are developed and benchmarked. The complete set of electromagnetic and fluid equations and the boundary conditions are presented. The transformation of fluid equations from a local reference frame, that is, moving with plasma or when the gas flow is zero, to a laboratory reference frame, that is, accounting for the gas flow, is discussed. The pressure range is extended down to 80 Pa by experimental measurements. The electron temperature decreases with pressure. The electron density depends linearly on power, and changes its behavior with pressure depending on the product of pressure and radial plasma size.

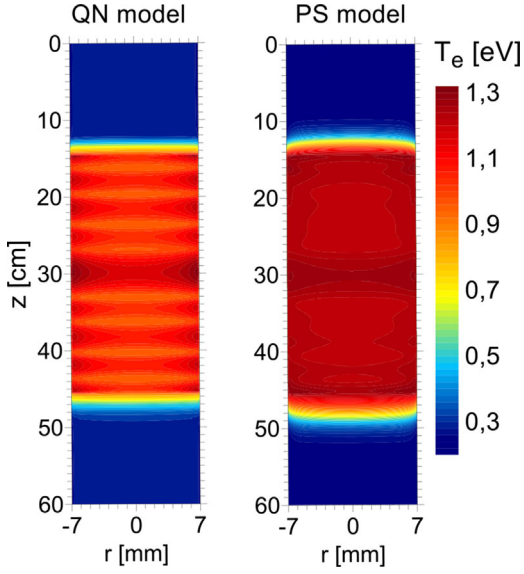

Dr. V. Georgieva, G. Chen, Dr. J. van der Mullen, Prof. M.-P. Delplancke-Ogletree
Université Libre de Bruxelles, École Polytechnique de Bruxelles, Service 4MAT, av. F.D. Roosevelt 50-CP 165/63, 1050, Brussels, Belgium
E-mail: violeta.georgieva@uantwerpen.be
Dr. V. Georgieva, A. Berthelot, Dr. St. Kolev, Prof. A. Bogaerts
Department of Chemistry, Research Group PLASMANT, University of Antwerp, Universiteitsplein 1, B-2610, Wilrijk-Antwerp, Belgium
Dr. T. Silva, Dr. N. Britun, G. Chen, Prof. R. Snyders
Université de Mons, ChIPS, av. Nicolas Copernic 1, 7000, Mons, Belgium
Dr. St. Kolev
Faculty of Physics, Sofia University, Blvd "James Bourchier" 5, 1164, Sofia, Bulgaria
Dr. W. Graef, Dr. D. Mihailova, Dr. J. van Dijk
Department of Applied Physics, Research Group EPG, Eindhoven University of Technology, P.O. Box 513, 5600 MB, Eindhoven, the Netherlands
Dr. T. Godfroid, Prof. R. Snyders
Materia Nova Research Center, av. Nicolas Copernic 1, 7000, Mons, Belgium

1. Introduction

Microwave (MW) induced discharges are well known for their high degree of non-equilibrium ($T_e >> T_{gas}$), the high level of applied energy absorption by plasma electrons, and relatively easy operation.[1–4] Based on the configuration reactors and the way of coupling the MW energy into the plasma, MW discharges can be divided into two general types: localized, that is, plasma created in resonant cavity reactors and plasma torches; and traveling-wave discharges, that is, surface-wave (SW) plasma columns.[1–4] They find application in a wide range of technology fields such as surface treatment,[5,6] material processing and (nanoparticle) synthesis,[7–9] plasma diagnostics,[10] plasma medicine (sterilization, skin treatment),[11–16] in atomic and molecular spectrometry,[17,18] and in dissociation of greenhouse gases.[19–21]

A SW sustained plasma, which is the topic of the present research, is created by electromagnetic (EM) waves propagating along the boundary between the plasma and a dielectric (usually a quartz tube).[1] The plasma SWs were discovered in the 1960's.[22] The first application of EM surface waves in the MW frequency range for sustaining plasma was developed by Moisan et al. in 1974.[23] Since then SW sustained discharges attracted significant attention due to their flexibility in terms of continuous or pulsed operation regimes, in a wide range of gas pressure (10^{-2}–10^5 Pa), applied frequency (300 MHz–10 GHz), and geometry size and shape.[1–4] A considerable amount of research has been done in a number of groups leading to a vast number of publications (cf. Refs.[1–21] and [23], presenting specific applications, Refs. [1–3] and [24–42], presenting analytical or modeling research, and Refs.[1–3] and,[43–52] presenting experimental or combined theoretical and experimental research). Just to mention some of the groups explicitly, we would like to refer to the pioneering work on the theory of SW propagation in guiding structure with different geometries and on the SW discharge applications done in Montreal, Lisbon, Sofia, Bochum, and Moscow, as well as in a number of collaborations among these groups and thus forming the solid basis for further SW sustained plasma research and applications.[1,3,11,12,19,23–25,27–35,37,43–45]

The principle of operation of a SW plasma source is based on the fact that the plasma is the only dielectric medium which can have a negative permittivity, ε_p, provided that the plasma frequency is larger than the applied wave frequency.[1] When bounded to a dielectric with positive permittivity ε_d and provided that $|\varepsilon_p| > \varepsilon_d$, plasmas can sustain surface wave propagation with evanescent fields on both sides of the boundary.[1,53] Propagation of the surface wave ionizes the plasma and the wave is sustained by the produced plasma. Hence, a mutual plasma-wave interaction is observed. The plasma column extends far away from the wave launcher. The energy from the wave is transferred to the plasma by the charged particles, especially by the electrons since they can follow the EM field and gain energy from it. The electrons transfer the energy to the heavy particles through collisions.

Examples of SW plasma generators are the surfatron, and the surfaguide launchers.[1–4] We have applied a surfaguide sustained discharge at intermediate pressure for plasma-catalytic greenhouse gas conversion into valuable chemicals.[21] Such an application requires careful investigation of the plasma column in order to achieve optimal dissociation rates of molecular species as well as optimal corresponding energy efficiency. Experimental measurements are not always possible at different positions of the plasma tube or on the catalytic surface, because of the solid metallic parts surrounding the set-up in order to prevent microwave energy leakage (see below for the description of the experimental set-up in Section Experimental Set-Up and the Computational Domain and Refs. [21,47]). Therefore, computer modeling of the plasma region can bring a valuable insight into the process. Understanding the plasma-wave interplay in the relatively simple Ar chemistry case is a first step towards understanding complex chemical plasmas in future.

The plasma column in SW discharges is non-uniform both in the radial and axial direction. The strong coupling of the wave and the plasma requires considerable computational resources even when a number of simplifications are applied. Initially, an approach of dividing the problem into two 1D problems was developed. The plasma is divided into thin slabs in the axial direction, assuming that the local axial gradients are negligible compared to the corresponding radial gradients.[24,25] The radial distribution of the plasma parameters and the wave propagation characteristics are obtained from the plasma maintenance equations and the wave-field equation for given discharge operating conditions and power delivered per unit length at a given axial position. Then the attenuation characteristic of the wave is found. The axial distribution of the power density is calculated from the wave energy balance equation. Merging the solution for each plasma slab allows determining the spatial distributions.[24,25] Next, the kinetics of the SW discharges was investigated which resulted in similarity laws.[26,27] Further, the attention was turned again to the wave properties, which particularly determine the waveguided plasma properties.[28,29] Analyzing the behavior of the space damping rate of the wave, an analytical solution for the axial distribution of the electron density was found.[28] The theory of the surface wave propagation and wave- plasma interaction are presented in detail in Refs. [1,3] and [29]. Other simplified approaches have also been applied: (i) considering a 1D problem in the axial direction, and assuming uniformity in the radial direction[30–32] or applying a radial profile of Bessel-type of

the electron density, which is obtained from an analytical solution of the electron density balance equation[33]; (ii) calculation of the electron energy distribution function (EEDF) from the Boltzmann equation[34]; (iii) applying a collisional radiative model (CRM) for plasma production in a uniform EM field[35]; (iv) coupling the CRM to the EM field equations in 1D (axial or radial) models.[36–38] More elaborated, self-consistent, 2D models solving self-consistently Maxwell's equations describing the EM field and the set of plasma fluid equations in ambipolar diffusion approximation and neglecting sheaths, have been developed using academic or commercial plasma modeling frameworks. [39–42] These models were applied to atmospheric pressure cylindrical (surfaguide or surfatron)[40,41] and to intermediate pressure coaxial microwave discharges.[42] The self-consistent solution of the plasma-wave equation set in 2D gives direct information on the plasma characteristics and electromagnetic field space distributions and reduces considerably the assumptions that need to be made when the problem is considered in 1D. Moreover, adding the heavy particle energy transport equation to the set of equations is another advantage of the 2D models. Therefore, the 2D models are an important step in the development of the SW sustained discharge modeling.

Despite its limitations, the ambipolar approximation has been successfully applied in intermediate pressure regimes.[16,36,42,54] A model that resolves the space-charge sheath region has also been developed, however, it considers only the radial description, that is, 1D model.[38] Further elaboration of the 2D models is the consideration of a gas flow,[39–41] which introduces additional complexity in the system of the fluid equations as it will be explained below in the model description section.

In this paper, we present and compare two 2D self-consistent models of microwave surfaguide discharges taking the gas flow into account and we extend the simulation pressure range by experimental measurements. The applied frequency is 2.45 GHz, the pressure is in the range of 80–2667 Pa, and the applied power varies from 50 to 200 W in the simulation and experiment. The choice of the pressure range is based on the application of the microwave discharges for CO_2 dissociation.[21] In addition, we found that the investigation of Ar discharges sustained by a surfaguide wave launcher in the range 300–3000 Pa is scarce in the literature.[26]

One of the developed models assumes infinitely thin sheaths and applies the ambipolar diffusion approximation. The other model resolves the sheaths by solving Poisson's equation.

An important classification parameter to analyze the different plasma sources is the pressure-radius pR product.[3] Increasing the value of this product leads to changes in the plasma behavior with respect to the nature of the ionization mechanism, the role of ambipolar diffusion versus volume recombination.[3,41,55,56] and the coupling to the electric field. According to the classification,[3,41] the main electron loss mechanism is ambipolar diffusion for pR (Pa mm) in the range of 10–1300. The next regimes are the transition region when volume recombination (1300–2600) and molecular assisted recombination (2600–2×10^4) start playing a role. The main electron production mechanism in the three regimes is step-wise ionization.[3,41]

For the plasma source under study, pR is in the range 700–2×10^4 Pa mm, which implies that stepwise ionization, volume recombination, and molecular assisted recombination have to be taken into account. Therefore, the description of the Ar chemistry, that is, the different species and the list of transitions between them, is of considerable importance for reliable calculation results. At the same time, the number of followed species should be kept limited in order to achieve a reasonable CPU time. We consider a set of Ar chemistry consisting of Ar neutrals, electrons, the atomic Ar^+ and molecular Ar_2^+ ions and two excited states grouping the 4*s* and 4*p* levels each, and an exhaustive list of reactions between the species. The set was previously applied for the simulation of a gliding arc discharge[57] and is presented in the Supporting Information.

The developed simulation models have pressure limitations. When the pressure decreases, the mean free path of the electrons increases and at 100 Pa it is calculated to be 4.5 mm (see Section Plasma Fluid Equation Set), which is comparable with the radius (7 mm) of the plasma tube. Therefore, the lowest pressure limit at which the solution is stable was found to be 200 Pa. The results from the models are extended with measurements of the plasma characteristics of the modeled set-up. Using a self-absorption method associated to optical emission spectroscopy (OES),[58] the metastable argon density and electron temperature, and the electron density are evaluated in the range 80–170 Pa.[59] The intensity of the excited Ar atom emission decreases whit increasing pressure similarly to the reported measurements in literature.[49,52] Experimentally, we found that the maximum pressure at which the optical signal is strong enough to define the Ar(4*s*) group density is 170 Pa. The gas temperature is measured by adding N_2 to the Ar plasma.[60] The modeling and experimental results are also compared with measurements, available in the literature, in Ar surfaguide[26,37] and surfatron[49,50] discharges at the position where the wave is launched and for similar operating conditions.

The influence of the applied power and pressure on the plasma characteristics is investigated both by simulations and by measurements.

The paper continues with a description of the experimental set-up and the corresponding simulation domain (Section Experimental Set-Up and the

Computational Domain), a presentation of the two 2D models (Section Description of the Models) and of the plasma diagnostics methods used in the experimental measurements (Section Plasma Diagnostics). The results are presented and discussed in Section Results and Discussion. Finally, conclusions are given in Section Conclusion.

2. Experimental Set-Up and the Computational Domain

The experimental set-up for the microwave plasma generation is shown in Figure 1. Symmetric surface waves are launched by a surfaguide operating at 2.45 GHz in the continuous regime. The discharge is generated in a quartz tube with a 7 mm inner radius R_0, surrounded by a polycarbonate tube with a 16 mm inner radius. The quartz and polycarbonate tubes have each 3 mm thickness. The inner tube is cooled by an oil flow at 10 °C. The metallic grid, which surrounds the plasma tubes and forms a Faraday cage, has a radius of 50 mm. There are two metal rings which confine the electromagnetic field in a region of 31 cm along the discharge tube (see also Figure 2 below, where the corresponding computational domain is shown). The center of the quartz tube is positioned in the waveguide gap. The gas mixture injected from the top of the system is regulated by electronic mass flow controllers. Further details of the experimental surfaguide system used in the present research can be found in ref.[47] The operating conditions under study are the following: pressure range 80–2667 Pa, applied power range 50–200 W, and a flow rate of 125 sccm.

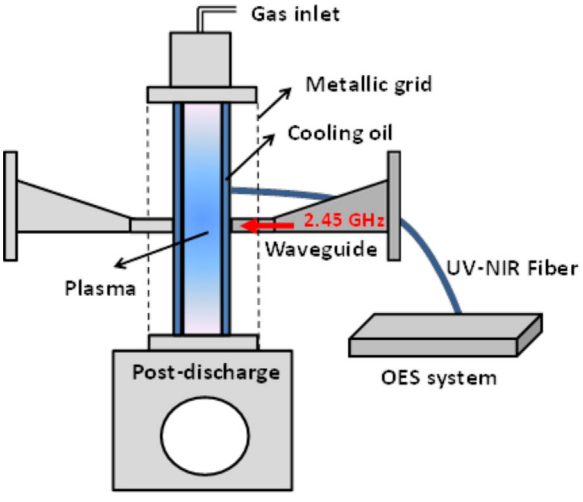

Figure 1. Schematic representation of the surface-wave microwave set-up.

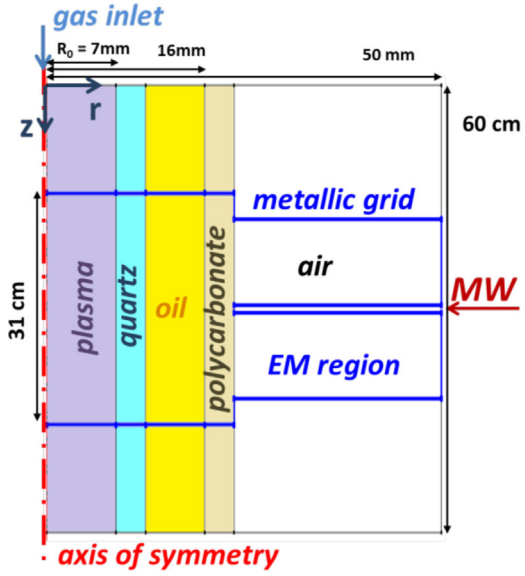

Figure 2. 2D axisymmetric computational domain. The metal boundaries are drawn in blue and confine the computational EM region. The plasma region is located in the inner quartz tube and is coloured purple.

The description of surface waves propagating at the plasma-dielectric boundary requires, generally speaking, a 3D approach. It is found that the product of the applied frequency and the plasma tube radius defines the propagation mode of the surface wave.[1,44] At the conditions under study, this product is 1.715 GHz.cm and hence the surfaguide launches symmetric surface waves propagating in transverse magnetic (TM) mode, that is, azimuthally symmetric ($m = 0$) waves. Therefore, taking into account also the cylindrical symmetry of the plasma tube, we can describe the system by a 2D axisymmetric model.

The computational domain corresponding to the experimental set-up is presented in Figure 2. In the developed models, the fluid description of the plasma is coupled to a self-consistent solution of Maxwell's equations. Maxwell's equations are solved in the region called EM region. In Figure 2 this is given by the region surrounded by the blue lines denoting the metal boundaries (either a metal grid or metal rings at the plasma tube). The plasma fluid equations are solved in the plasma region, that is, the inner quartz tube (see Figure 2). The difference in the two models comes from the different descriptions of the plasma. In the first model the sheath is assumed infinitely thin and is neglected, thus assuming quasi-neutral plasma in the complete volume. This model will be referred to as quasi-neutral (QN) model further in the text. It is developed in the modeling framework PLASIMO.[39,41,42,61–63] The second model considers the formation of the sheath next to the tube wall, and hence it is referred to as plasma bulk-sheath (PS) model below. The PS model is developed within the commercial software COMSOL Multiphysics® ref.[64]

3. Description of the Models

We shall start with the features common to both models. The following assumptions apply:

1. The EEDF is assumed to be Maxwellian ref.[65]

   When the EEDF is close to the Maxwell-Boltzmann distribution, the average electron energy $\langle\varepsilon\rangle$ is proportional to the electron temperature, T_e : $\langle\varepsilon\rangle = 3k_BT_e/2$, where k_B is the Boltzmann constant in $\mathrm{J\,K^{-1}}$ and T_e is expressed in K. Very often the electron energy is expressed in eV ($1\,\mathrm{eV} = 1.6022 \times 10^{-19}\,\mathrm{J}$). Hence, the relation between the average electron energy and electron temperature becomes[66]

$$\langle\varepsilon\rangle[eV] = \frac{3}{2}kT_e[eV], \tag{1}$$

   where k is 1 when the electron temperature is expressed in eV and is often omitted.

2. All heavy species are assumed to have a Maxwellian distribution.
3. The plasma is characterized by two temperatures: the electrons have a temperature T_e and all heavy particles have one temperature T_h. In general $T_e \neq T_h$.
4. We consider a weakly ionized collisional plasma, which means that the collision frequency of electrons and ions with neutral atoms greatly exceeds the collision frequency of these particles with one another. Hence the electron-electron (e-e) and ion-ion collisions are not considered in the models. However, the e-e collisions are taken into account within the solution of the BE in Bolsig + [67] and thus in the calculation of the e-Ar reaction rate coefficients.
5. The flow is laminar, that is, relatively low values of the Reynolds number.
6. In the QN model, we consider a stationary case, that is, zero time-derivatives of all plasma characteristics. In the PS model the time-derivatives are not neglected. The time steps are calculated by COMSOL based on the convergence of the solver for each time step (i.e., if convergence, the time step is reduced, otherwise the time step is increased). Since the PS model runs until a steady state solution is found, the time dependence has little influence and hence, we may assume that in both models the solution is time independent.

3.1. Electromagnetic Field Equations

Both models solve the same set of equations describing the surface electromagnetic waves. From Maxwell's equations the curl equations (Maxwell-Ampere's and Faraday's laws) predict the wave propagation. Therefore, these two equations are solved in the EM region in order to calculate the electric, $\vec{E}$, and magnetic, $\vec{H}$, field vectors. For symmetric surface waves propagating in TM mode, the non-zero electric and magnetic field components in a cylindrical coordinate system (r, φ, z) are E_r, E_z, and H_φ, respectively, with the wave-vector $\vec{k}$ directed along the z-axis.[1]

The electromagnetic field equations are solved in the frequency domain, assuming that all harmonic components above the fundamental frequency can be neglected, that is, assuming a sinusoidal signal. Therefore, the phasor notation $\mathcal{F}(r,\varphi,z,t) = Re[F(r,\varphi,z)\exp(i\omega t)]$ is used and the time dependency is removed from Maxwell's equations,[41,68] giving

$$\nabla \times \vec{E} = -i\omega\mu_0\vec{H}, \tag{2}$$

$$\nabla \times \vec{H} = \vec{J} + i\omega\varepsilon_r\varepsilon_0\vec{E}. \tag{3}$$

The dielectric permittivity ε_r is a scalar, ε_0 and μ_0 are the permittivity and permeability of free space, ω is the wave angular frequency, and i is the imaginary unit, $i^2 = -1$. The relative magnetic permeability of the waveguide system is taken as 1.[29] The ion mobility is low compared to the electron mobility, so we can neglect the ion current and hence the total current density is equivalent to the electron current density. The electron current density $\vec{J}$ is calculated from Ohm's law introducing a complex conductivity $\hat{\sigma}$.[41,68]

$$\vec{J} = \hat{\sigma}\vec{E}, \tag{4}$$

$$\hat{\sigma}(r,z) = \frac{e^2}{m_e}\frac{n_e(r,z)}{[\nu_m(r,z) + i\omega]}. \tag{5}$$

where $n_e(r,z)$ is the electron number density, m_e and e are the electron mass and charge, respectively, and $\nu_m(r,z)$ is the total elastic momentum transfer frequency between electrons and heavy particles. The equation of the complex conductivity is valid in a cold plasma approximation, which means that the electron thermal velocity is small compared to the wave phase velocity.[69] Surface waves were obtained only as slow waves, and hence, the phase velocity is smaller than the light speed $c = 1/\sqrt{\varepsilon_0\mu_0}$ in vacuum due to the interaction with the surrounding dielectric with a relative, or dielectric, permittivity ε_r.[3] The dielectric permittivity of quartz is close to 4, hence the wave phase velocity $c/\sqrt{\varepsilon_r}$ is $1.5 \times 10^8\,\mathrm{m\,s^{-1}}$. The electron thermal velocity under investigation is in the order of 10^5–$10^6\,\mathrm{m\,s^{-1}}$.

Combining equation (2), (3), and (4), the wave equation for the electric or magnetic field in the general three-

dimensional form can be readily derived. For the surface waves in TM mode, we solve the following system of equations for the three non-zero components E_r, E_z, and H_φ [41,68]

$$\frac{\partial E_z}{\partial r} - \frac{\partial E_r}{\partial z} = i\omega\mu_0 H_\varphi, \tag{6}$$

$$i\frac{\partial H_\varphi}{\partial z} = \omega\varepsilon_0\hat{\varepsilon}_r E_r, \tag{7}$$

$$i\frac{1}{r}\frac{\partial rH_\varphi}{\partial r} = -\omega\varepsilon_0\hat{\varepsilon}_r E_z, \tag{8}$$

where $\hat{\varepsilon}_r = \varepsilon_r - \frac{i\hat{\sigma}}{\varepsilon_0\omega}$ is defined as a complex permittivity, ε_r being 1 for plasma. The other materials are described only by the real component, ε_r, which is 1 for air, 3.96 for quartz, 2.75 for oil, and 2.8 for the polycarbonate material.

The following *boundary conditions* (BCs) apply for the electric and magnetic fields:

(i) At the axis of symmetry: E_r and $H_\varphi = 0$.
(ii) At material interfaces:

a. Between different dielectric materials and at the plasma-dielectric boundary: continuity of the tangential components E_z and H_φ, that is, $\frac{\partial E_z}{\partial r} = 0$ and $\frac{\partial H_\varphi}{\partial r} = 0$. In addition, there is no free surface charge, which means that for the displacement electric field $\vec{D}_1 = \varepsilon_r\vec{E}$ the following BC applies: $\left(\vec{D}_1 - \vec{D}_2\right)\vec{n} = 0$. Hence, the normal component of the electric field, which is E_r in our case, satisfies $\epsilon_{r1}E_{r1} = \epsilon_{r2}E_{r2}$ at both sides of the boundary between materials with relative permittivity ε_{r1} and ε_{r2}, respectively.

b. Between a dielectric and a metal: a perfect electrical conductor BC is applied, which means that the tangential component is 0. We assume that the metal is a perfect conductor and the electric field is reflected at the metal boundaries. Therefore the corresponding tangential component of the electric field, which is E_z along a boundary parallel to the z-axis and E_r along a boundary parallel to the r-axis, is set to 0.

(iii) At the waveguide gap: an excitation BC, which specifies an initialization value of E_z. The scale of the incoming electric field is arbitrary and it is iteratively re-scaled to match the input and the absorbed power. The absorbed power density Q_{Ohm} (W m^{-3}) is computed as

$$Q_{Ohm} = \frac{1}{2}Re\left(\vec{J}\cdot\vec{E}\right) = \frac{1}{2}Re(\hat{\sigma})\left|\vec{E}\right|^2. \tag{9}$$

The manuals of PLASIMO[63] and COMSOL[64] supply further information on the equations and the numerical procedure for solving them.

Here we present the deposited power density (Figure 3) and the electric field (Figure 4) calculated by both models when we assume as input uniform plasma properties and momentum transfer collision frequency in the entire plasma volume (so called 1-step run).

Figure 3 shows a good agreement in the power density absorbed in the plasma region calculated by the two models. The maximum value in front of the wave-guide gap is calculated to be 6.73×10^7 and 6.27×10^7 W m^{-3} in the QN and PS models, respectively. As it is expected, the power is mainly deposited along the plasma- dielectric boundary. A good agreement is found also in the calculated EM field components. Figure 4 shows E_z (a) and E_r (b) in the plasma region calculated by both models. The

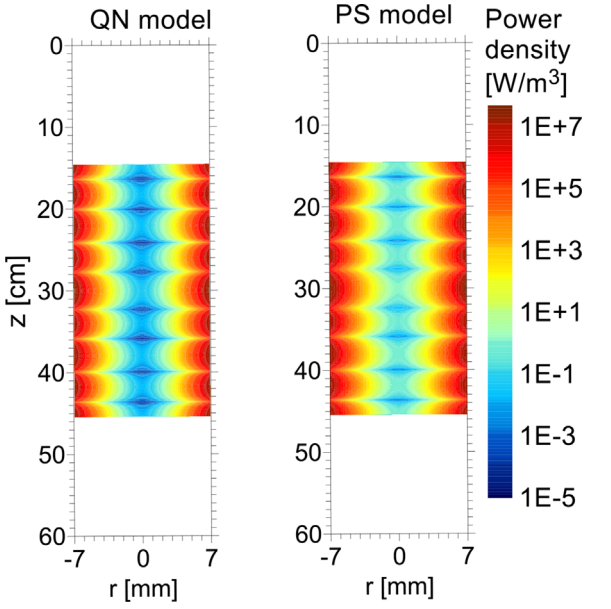

Figure 3. Power density deposition in the plasma region calculated in the QN model and in the PS model by one-step run with the following input data: uniform electron density of 10^{20} m^{-3}; uniform electron temperature of 13,000 K (1.12 eV), uniform gas temperature of 1000 K, applied power of 100 W, pressure of 1000 Pa, and a gas flow rate of 125 sccm. The coloured scale is the same for the two plots.

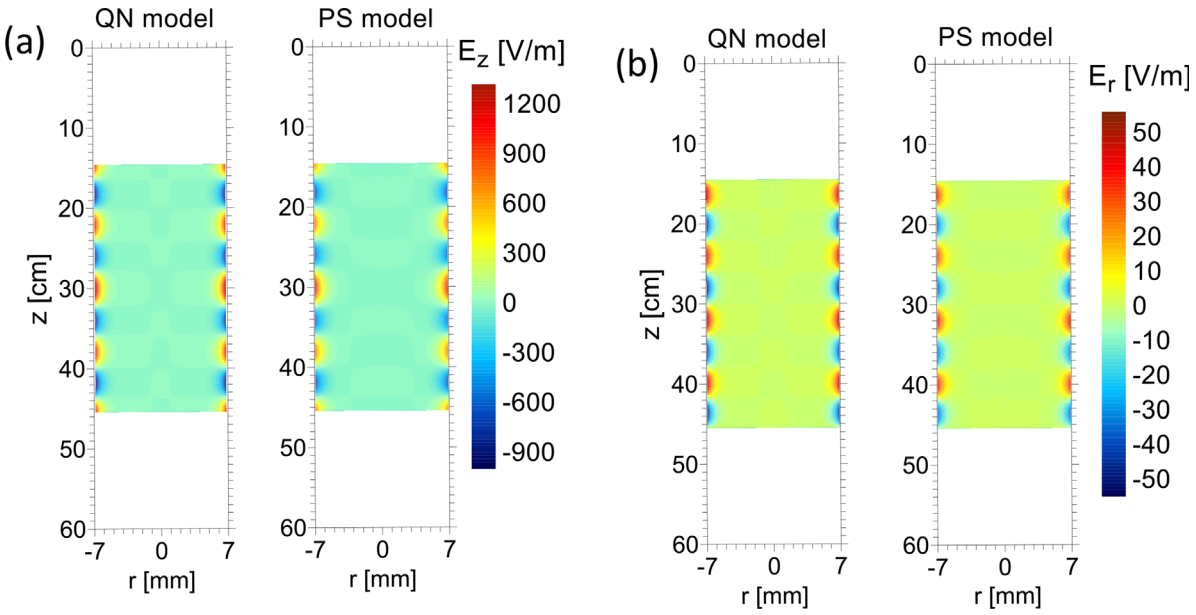

Figure 4. The axial E_z (a) and radial E_r (b) components (real values) of the electric field calculated in the QN and PS models. The input data and operating conditions are the same as in Figure 3.

electric field does not penetrate deeply as is expected in the case of surface wave propagation.[1,3]

3.2. Plasma Description in Local and Laboratory Reference Frames

Plasmas contain a very large number of particles interacting with each other. Therefore, one approach to describe such a system is the statistical approach. The plasma is considered as a continuum medium and the equation of motion is solved for a system of particles considered as a whole. From classical mechanics we know that the instantaneous state of a particle can be specified by its position $\vec{r}(x_1, x_2, x_3)$ and velocity $\vec{v}(v_{x_1}, v_{x_2}, v_{x_3})$. If we consider a finite volume element $d^3r d^3v$, and the number of particles type α at a given time t is $d^6N_\alpha(\vec{r}, \vec{v}, t)$ in this volume element, the distribution function $f_\alpha(\vec{r}, \vec{v}, t) = \frac{d^6N_\alpha(\vec{r},\vec{v},t)}{d^3r d^3v}$ is defined as the density of particles α in the 6d phase space at time t. [69,70] The macroscopic variables such as number density, flow velocity, kinetic pressure, thermal energy flux, and so on, can be considered as average values of the particle physical quantities involving the collective behavior of large number of particles. The number density $n_\alpha(\vec{r}, t)$ is defined as the number of particles, $d^6N_\alpha(\vec{r}, \vec{v}, t)$, inside the volume element d^3r of the configuration space, irrespective of velocity [69]

$$n_\alpha(\vec{r}, t) = \frac{1}{d^3r}\int_v d^6N_\alpha(\vec{r}, \vec{v}, t) = \int_v f_\alpha(\vec{r}, \vec{v}, t)d^3v. \quad (10)$$

The macroscopic value of a particle physical property $\chi(\vec{r}, \vec{v}, t)$ can be found by multiplying $\chi(\vec{r}, \vec{v}, t)$ with the number of particles integrating over the velocity space and dividing by the number of particles inside the volume element d^3r,which is $n_\alpha(\vec{r}, t)d^3r$.

$$\langle\chi(\vec{r}, \vec{v}, t)\rangle_\alpha = \frac{1}{n_\alpha(\vec{r}, t)}\int_v \chi(\vec{r}, \vec{v}, t)f_\alpha(\vec{r}, \vec{v}, t)d^3v. \quad (11)$$

For example, for $\chi(\vec{r}, \vec{v}, t) \equiv 1$ we obtain the number density, that is, Equation (10); for $\chi(\vec{r}, \vec{v}, t) \equiv \vec{v}$, we obtain the macroscopic average or flow (directed) velocity $\vec{u}_\alpha(\vec{r}, t)$ of particles type α. Therefore, it is necessary to know the distribution function $f_\alpha(\vec{r}, \vec{v}, t)$ in order to calculate the macroscopic variables. The distribution function can in principle be found by solving the Boltzmann equation (BE). Its general form is [69]

$$\frac{\partial f_\alpha}{\partial t} + \vec{v}\cdot\nabla f_\alpha + \frac{\vec{F}}{m_\alpha}\nabla_v f_\alpha = \left(\frac{\delta f_\alpha}{\delta t}\right)_{coll}, \quad (12)$$

where $\left(\frac{\delta f_\alpha}{\delta t}\right)_{coll}$ is the rate of change of f_α due to collisions, $\vec{F}$ is the microscopic force acting on each particle with mass m_α. The left side of Equation (12) is the total derivative of $f_\alpha(\vec{r}, \vec{v}, t)$ with respect to time. If there are no collisions, the total derivative is 0. Hence the BE is a statement of conservation of density of particles α in the phase space.

A plasma is a mixture of various species α (α denoting electrons, ions, or neutrals in ground or excited states) and

apart from the specific properties given above we may also define quantities for the plasma bulk. For example, the total number density is defined by: $n = \sum_\alpha n_\alpha$; the average mass $m = \frac{1}{n}\sum_\alpha n_\alpha m_\alpha$; the average mass density $\rho_m = \sum_\alpha n_\alpha m_\alpha = \sum_\alpha \rho_{m\alpha}$, and the average mass or bulk flow velocity of the plasma, $\vec{u}$, by

$$\vec{u} = \frac{1}{\rho_m}\sum\nolimits_\alpha \rho_{m\alpha}\,\vec{u}_\alpha \tag{13}$$

The particle velocity can be presented with respect to the particle flow velocity, $\vec{u}_\alpha$, or with respect to the plasma (gas) flow velocity, $\vec{u}$

$$\vec{v} = \vec{u}_\alpha + \vec{c}_\alpha, \tag{14}$$

$$\vec{v} = \vec{u} + \vec{c}_{\alpha 0}, \tag{15}$$

where $\vec{c}_\alpha$ is the random or thermal velocity, and $\langle \vec{c}_\alpha \rangle_\alpha = 0$; $\vec{c}_{\alpha 0}$ is the alternative random particle velocity relative to $\vec{u}$.[69] The average value of $\vec{c}_{\alpha 0}$ is the mean velocity of each particle type α, called the diffusion velocity $\vec{w}_\alpha = \langle \vec{c}_{\alpha 0} \rangle_\alpha$,, and has the meaning of the average particle velocity in a reference frame moving with the plasma. Thus the relation between the average particle velocity, $\vec{u}_\alpha$, and the total plasma flow velocity, $\vec{u}$, is given by

$$\langle \vec{v} \rangle_\alpha = \vec{u}_\alpha = \vec{u} + \vec{w}_\alpha \tag{16}$$

From Equation (13) we have $\rho_m \vec{u} = \sum_\alpha \rho_{m\alpha}\,\vec{u}_\alpha$

$$= \sum\nolimits_\alpha \rho_{m\alpha}\,(\vec{u} + \vec{w}_\alpha)$$

and hence

$$\sum\nolimits_\alpha \rho_{m\alpha}\,\vec{w}_\alpha = 0 \tag{17}$$

For a collision-dominated plasma, it is more convenient to consider the particle velocities in a local frame of reference moving with the average velocity of the plasma.[69,70] In many books on plasma physics, the governing equations are derived in a reference frame moving with the plasma or considering that there is no plasma (gas) flow.[66,69,70] However, often the plasma (gas) flow velocity cannot be neglected in comparison with the diffusion velocity, as will be discussed in Section Pressure range extension by experimental measurements. The transformation of the governing equations from one velocity representation to the other (i.e., the same as transforming the reference frames from a local reference frame, moving with the plasma, to a laboratory reference frame, in which the plasma moves with $\vec{u}$) is not always trivial. In addition, on the one hand, the transport plasma properties are governed by the transport of the species and their energy by different types of diffusion (due to external fields, density gradients or temperature gradients). On the other hand, an important plasma property is the absolute temperature of species, which is a measure for their thermal energy and is expressed by their velocity component due to random, chaotic, motion. Therefore, we present the general form of the transport equations in both velocity representations in the Appendix, Section Transport equations in local and laboratory reference frames.

3.3. Plasma Fluid Equation Set

3.3.1. Specific Density Balance Equation

QN model:

$$\vec{\nabla}.(n_\alpha \vec{u}) - D_\alpha \nabla n_\alpha = \left[\frac{\delta(n_\alpha)}{\delta t}\right]_{coll}, \tag{18}$$

which is Equation (A3) from the Appendix if neglecting $\partial/\partial t$ and applying Fick's law for the neutral diffusion flux and ambipolar diffusion approximation for the ions. It is solved for $(N-2)$ types of particles. The electron density is equal to the sum of the (positive) ion densities: $n_e = \sum_i n_i$. Effective diffusion coefficients are used for the neutral species in excited state and the ambipolar diffusion coefficient D_A [Equation (A39) from the Appendix] for the ions. Further information on the diffusion coefficients used in the QN model can be found in [41,68].

PS model:

$$\frac{\partial n_\alpha}{\partial t} + \vec{u}\cdot\nabla n_\alpha + \vec{\nabla}\cdot\vec{\Gamma}_{\alpha,dif} = \left[\frac{\delta(n_\alpha)}{\delta t}\right]_{coll}, \tag{19}$$

which is Equation (A3) from the Appendix if neglecting the term $n_\alpha \vec{\nabla}.\vec{u}$. Equation (19) is solved for $(N-1)$ types of particles. The electron and ion diffusion fluxes $\vec{\Gamma}_{\alpha,dif} = n_\alpha \vec{w}_\alpha = n_\alpha Z_\alpha \mu_\alpha \vec{E} - \nabla(D_\alpha n_\alpha), \alpha = e, i,$, are calculated based on the drift-diffusion approximation, applying Equation (A36) and (A37). The electron mobility is calculated from BOLSIG+.[67] The mobility for the ions is taken from[72]

$$\mu_{Ar^+} = \frac{1.01.10^5}{p}\frac{T_h}{273.16} \times 1.52.10^{-4}\,\mathrm{m^2V^{-1}s^{-1}}, \tag{20}$$

$$\mu_{Ar_2^+} = 1.2 \times \mu_{Ar^+}. \tag{20a}$$

The electron and ion diffusion coefficients are calculated from Einstein's relation.

The Ar(4*s*) and Ar(4*p*) diffusion coefficients are adopted from[73]

$$D_{Ar(4p)} = D_{Ar(4s)} = \frac{1.16.10^{20}}{n_{Ar}} \left(\frac{T_h}{300}\right)^{\frac{1}{2}} \mathrm{m}^2 \cdot \mathrm{s}^{-1}. \quad (21)$$

Both models: The neutral gas (Ar atoms in ground state) density is found from the ideal gas law. The diffusion of neutral species in excited state is described by Fick's law (see Equation [A41] in the Appendix). The contribution of diffusion due to the temperature gradients is neglected. The net production of species α due to different collisional-radiative processes and reactions is calculated based on the Ar chemistry set presented in the Supporting Information.

3.3.2. Specific Energy Balance Equations

a. Electron energy balance equation

QN model

$$\frac{3}{2}\vec{\nabla}.(n_e k_B T_e \vec{u}) + n_e k_B T_e \vec{\nabla}.\vec{u} + \nabla(-\lambda_e \nabla(k_B T_e)) = Q_{Ohm} - Q_{eh}^{inel} - Q_{eh}^{el}. \quad (22)$$

The electron energy balance is derived from Equation (A13a) from the Appendix taking into account 0 time-derivatives. The partial pressure is given by the equation of state for an ideal gas, Equation (A16). The Ohmic heating, Q_{Ohm}, is calculated by Equation (9) because the electron current density is equivalent in both velocity representations when the plasma is neutral (see Equation [A28] from the Appendix). The right-hand side of Equation (A13a) is the loss of electron energy in elastic and inelastic collisions, Q_{eh}^{elas} and Q_{eh}^{inel}, respectively. The terms $(p_e \vec{w}_e + n_e \varepsilon_e \vec{w}_e)$ in the electron heat flux in Equation (A32), which are due to the transformation to the laboratory reference are equal to $\left(-\frac{5}{2} k_B T_e D_A \nabla n_e\right)$. The expression can be easily found by applying Equation (A11), (A16), and (A38) from the Appendix. This term is neglected in the QN model. Using that $\lambda_e = \frac{5}{2} D_e n_e$, the electron heat flux in case of gas flow and ambipolar diffusion approximation is equal to

$$\vec{q}_e{}' = -\frac{5}{2} D_e n_e \nabla(k_B T_e) - \frac{5}{2} k_B T_e D_A \nabla n_e = -\frac{5}{2} n_e k_B T_e \left(D_e \frac{\nabla T_e}{T_e} + D_A \frac{\nabla n_e}{n_e}\right). \quad (23)$$

Typically in plasma $\frac{\nabla T_e}{T_e} \ll \frac{\nabla n_e}{n_e}$.[70] As discussed in the Appendix, Section Ambipolar diffusion approximation for charged particles, $D_e \gg D_A$. Therefore, it is difficult to estimate if the second term in the heat flux is justified to be neglected. Further investigations are foreseen.

The electron thermal conductivity λ_e is calculated according to Devoto (third order approximation).[74] The energy gain or loss through inelastic collisions Q_{eh}^{inel} is obtained from[41,68]

$$Q_{eh}^{inel} = \sum\nolimits_l R_l \Delta\varepsilon_l, \quad (24)$$

where R_l is the rate constant for the inelastic collision l, and $\Delta\varepsilon_l$ is the average energy exchange per collision. The energy lost through elastic collisions Q_{eh}^{el} is obtained from[41,68]

$$Q_{eh}^{el} = \sum_{s \neq e} \frac{3}{2} n_e \nu_{es} \frac{2m_e}{m_s} k_B (T_e - T_h), \quad (25)$$

where ν_{es} is the elastic momentum transfer between electrons and species s.

PS model:

$$\frac{\partial}{\partial t}(n_\varepsilon) + \nabla.\vec{\Gamma}_\varepsilon + \vec{\Gamma}_{e,dif}.\vec{E} = -Q_{eh}^{inel} - Q_{eh}^{el} - (\vec{u}.\nabla)n_\varepsilon. \quad (26)$$

It is obtained from Equation (A13a) from the Appendix. The electron heat flux vector, Equation (A32), can be transformed to

$$\vec{q}_e + p_e \vec{w}_e + n_e \varepsilon_e \vec{w}_e = -\frac{5}{3} e n_\varepsilon \left(\mu_e \vec{E}\right) - \frac{5}{3} e \nabla(D_e n_\varepsilon), \quad (27)$$

where $n_\varepsilon = n_e \varepsilon_e$ is the electron thermal energy density expressed in [eV m^{-3}]. Equation (A36), (A42), and (A43) and the relation $\frac{3}{2} p_e = \frac{3}{2} n_e k_B T_e = e n_e (\varepsilon_e[eV])$ are used in the derivation of Equation (27). The electron energy flux $\vec{\Gamma}_\varepsilon$ is introduced

$$\vec{\Gamma}_\varepsilon = -n_\varepsilon \left(\mu_\varepsilon \vec{E}\right) - \nabla(D_\varepsilon n_\varepsilon), \quad (28)$$

where $\mu_\varepsilon = \frac{5}{3}\mu_e$ and $D_\varepsilon = \frac{5}{3} D_e$. Hence the term $\vec{\nabla}.\left(\vec{q}_e + p_e \vec{w}_e + n_e \varepsilon_e \vec{w}_e\right)$ in Equation (A13a) is equal to

$$\vec{\nabla} \cdot \left(\vec{q}_e + \frac{5}{2} p_e \vec{w}_e\right) = e \nabla \cdot \vec{\Gamma}_\varepsilon \quad (29)$$

The Ohmic heating, which is the same as in Equation (22), is expressed by the electron diffusion flux $\vec{\Gamma}_{e,dif} = n_e \vec{w}_e$

$$Q_{ohm} = -n_e e\vec{w}_e \cdot \vec{E} = -e\vec{\Gamma}_{e,dif} \cdot \vec{E}. \quad (30)$$

Finally, applying Equation (27)–(30), the electron energy balance equation has the form presented in Equation (26). Solving it, we find the electron energy density n_ε, and hence the average electron energy ε_e. The electron temperature, T_e, is calculated from the average electron energy by Equation (2). The difference with the electron energy balance equation solved in the QN model, that is, Equation (22), is that in the PS model the term in the heat flux vector accounting for the transformation to a laboratory reference frame in case of a plasma flow is taken into account. The other difference between the two equations is the first term considering the time dependence. However, as discussed above, the solution in the PS model is steady-state, and neglecting time dependence in the QN model is completely justified (see Section Validation of the assumptions in the QN model below). Therefore, we consider that accounting for the time variation in the PS model does not influence the solution for the conditions under study.

b. Heavy particle energy balance equation

QN model:

$$\vec{\nabla}.\left(C_{p,h}T_h\vec{u}\right) - \vec{u}.\nabla p_h + \nabla(-\lambda_h \nabla k_B T_h) = Q_{eh}^{elas} + Q_{h*h}^{inel}, \quad (31)$$

The equation is derived based on the following steps. As mentioned in the list of approximations, all heavy particles are considered to have one temperature T_h and to have a Maxwellian energy distribution. Therefore, we solve one energy balance equation for the heavy particles by summing Equation (A13a) from the Appendix over all species except for the electrons and neglecting the time derivatives, the viscosity, and the ion current density.

$$\vec{\nabla} \cdot \left[\frac{3}{2}\left(\sum_{s\neq e} n_s\right)k_B T_h \vec{u}\right] + \left(\sum_{s\neq e} n_s\right)k_B T_h \vec{\nabla} \cdot \vec{u} + \nabla(-\lambda_h \nabla k_B T_h) - \frac{5}{2}\nabla\left(\sum_{s\neq e} k_B T_h D_s \nabla n_s\right) = Q_{eh}^{elas} + Q_{h*h}^{inel}, \quad (32)$$

where the subscript "h" refers to "heavy particles". The change of the energy is due to gain through elastic collisions with electrons, Q_{eh}^{elas}, and gain or loss through inelastic collisions with heavy particles, Q_{h*h}^{inel}, in which the internal energy is converted into heat.[39]

The contribution in the heat flux vector due to the transformation to a laboratory reference frame is neglected (the last term in the left-hand side of Equation (32)).

To make Equation (32) applicable for atoms and molecules, we use the volumetric heat capacity at constant volume: $C_{v,h} = \frac{1}{T_h}\sum_{s\neq e} E_s n_s$ in [J m^{-3} K^{-1}], where the internal energy per particle E_s is given by the number of degrees of freedom, f, and the energy associated to 1 degree of freedom: $\frac{1}{2}k_B T_h$: $E_s = f\frac{1}{2}k_B T_h$ f depends on the number of atoms in a particle. For a monoatomic particle, $f = 3$ (3 degrees of translational motion) and for a diatomic particle $f = 5$ (3 degrees of translational freedom + 2 degrees of rotational freedom). The volumetric heat capacity at constant pressure $p_h = \left(\sum_{s\neq e} n_s\right)k_B T_h$ is defined as: $C_{p,h}T_h = C_{v,h}T_h + \left(\sum_{s=i,n} n_s\right)k_B T_h$. Applying all definitions above, the heavy particle energy balance can be written in the form given in Equation (31).

The thermal conductivity coefficient λ_h is obtained based on ref.[75]

PS model:

$$\rho_m c_p \frac{\partial T_h}{\partial t} + \rho_m c_p \vec{u}.\vec{\nabla} T_h + \nabla(-\lambda_h \nabla T_h) = Q_{eh}^{elas} + Q_{eh}^{inel}, \quad (33)$$

where c_p is the specific heat capacity at constant pressure, $c_p T_h = c_v T_h + \rho_m R T_h$, and c_v is the specific heat capacity at constant volume in [J kg^{-1} K^{-1}].

Similar to the QN model, one energy balance equation is solved for all heavy particles and the contribution in the heat flux vector due to the transformation to a laboratory reference frame is neglected. The Equation (A13a) from the Appendix is summed over all species and the electron pressure is neglected. Therefore, the pressure of the heavy particles is assumed equivalent to the Ar gas pressure and the thermal conductivity and specific heat capacity at constant pressure of Ar gas are used for the values of λ_h and c_p, respectively (COMSOL[64] database). We apply the ideal gas law $p = nk_B T_h = \rho_m R T_h$, and express the internal energy by $\varepsilon = c_v T$.The terms containing $(\vec{\nabla} \cdot \vec{u})$ and the time dependence of $\vec{u}$ are neglected.

3.3.3. Continuity Equation for the Plasma

Both models solve Equation (A4) from the Appendix, neglecting the time-derivative in the QN model, in order to calculate the plasma (gas flow) velocity.

Plasma Process Polym **2017,** *14*, 1600185

3.3.4. Momentum Balance for the Plasma

Both models solve Equation (A9) from the Appendix, neglecting the time-derivative in the QN model, in order to define the total pressure. The viscosity tensor for the Ar gas is calculated based on Equation (A31).[68]

3.3.5. Poisson's Equation

It is solved in the PS model to obtain the plasma potential φ

$$\Delta\varphi = \frac{\rho}{\varepsilon_0}. \tag{34}$$

3.3.6. Boundary Conditions

The BCs for solving the system of the transport equations in both models are presented in Table 1. In addition, the specific BCs for each model are presented below.

QN model: The BC for the flux of the excited Ar atoms to the wall is found from[66]

$$\Gamma_s(R_0) = \gamma\frac{1}{4}n_s(R_0)\sqrt{\frac{8k_BT_h(R_0)}{\pi m_{Ar}}}, \tag{35}$$

where s denotes Ar(4s) or Ar(4p), γ is the sticking coefficient and is equal to 1, that is, all excited species are de-excited once reaching the quartz tube wall.

The BCs for the electron temperature and ion flux at the wall are derived from the Bohm sheath theory.[66,70] A sheath is formed next to the wall, and in that region the quasi-neutrality is not fulfilled. Since due to ambipolar removal the walls acquire a negative charge, the electric field in the sheath is directed towards the wall. The ions are accelerated in the pre-sheath to a velocity, which is equal to the Bohm velocity $v_{Bohm} = \sqrt{k_BT_e/m_i}$.[66] If the mean free path is much longer than the sheath width, which is in the order of the Debye length, all ions entering the sheath, reach the wall and we assume that they recombine at the wall. The mean free path $\lambda_i = 1/n_{Ar}\sigma_{Ar^+Ar}$ for the ions is calculated to be 4×10^{-3} mm, which is indeed greater than the calculated Debye length of 7.5×10^{-4} mm at 1000 Pa. The corresponding data at 100 Pa are 4×10^{-2} mm and 3.3×10^{-3} mm. Hence, the ion flux at the wall is defined from

$$\Gamma_i(R_0) = -D_A\frac{\partial n_i}{\partial r}|_{R_0} = n_i v_{Bohm}. \tag{36}$$

The electrons which enter the sheath can reach the wall only if their initial energy exceeds $e\Delta\phi$. This condition defines the electron flux at the wall by integrating over the velocity component normal to the wall and for electron energy exceeding the plasma potential.[70] Applying that the electron and ion densities are equal at the plasma bulk-sheath boundary layer, the electron flux in the absence of current towards the wall is[70]

$$\Gamma_e(R_0) = n_i(R_0)\sqrt{\frac{k_BT_e}{2\pi m_e}}\exp\left(-\frac{e\Delta\varphi}{k_BT_e}\right). \tag{37}$$

The potential difference $\Delta\varphi$ in the sheath is found from equating the ion and electron fluxes at the wall, that is, Equation (36) and (37),[70]

$$\Delta\varphi = \frac{k_BT_e}{e}\ln\sqrt{\frac{m_i}{2\pi m_e}}. \tag{38}$$

For the typical conditions under study ($T_e = 1.0$–1.4 eV see the results in the next section) the potential difference is calculated to be $5\div7$ V.

The BC for T_e at the plasma bulk-sheath boundary layer is found from[70]

Table 1. BCs for solving the system of transport equations in the QN and PS models.[a)]

Inlet	Outlet	Axis of symmetry	Tube wall
$\frac{\partial\psi^{b)}}{\partial z} = 0$	$\frac{\partial\psi}{\partial z} = 0$	$\frac{\partial\psi}{\partial r} = 0$	$T_h = 283K$
$\vec{n}.\overrightarrow{\Gamma_e} = 0$	$\vec{n}.\overrightarrow{\Gamma_e} = 0$	$\vec{n}.\overrightarrow{\Gamma_e} = 0$	$\vec{n}.\overrightarrow{\Gamma_e} = \frac{1}{2}v_{e,th}n_e$
$\vec{n}.\overrightarrow{\Gamma_\varepsilon} = 0$	$\vec{n}.\overrightarrow{\Gamma_\varepsilon} = 0$	$\vec{n}.\overrightarrow{\Gamma_\varepsilon} = 0$	$\vec{n}.\overrightarrow{\Gamma_\varepsilon} = \frac{5}{2}v_{e,th}n_\varepsilon$,
$u_z(r) = \frac{2\Phi}{\pi R_0^2}\left[1-\left(\frac{r}{R_0}\right)^2\right]^{c)}$	$\frac{\partial u_z}{\partial z} = 0$	$\frac{\partial u_z}{\partial r} = 0$	$u_z = 0$
$\frac{\partial^2 p}{\partial z^2} = 0$	$p = p_{pump}$	$\frac{\partial p}{\partial r} = 0$	$\frac{\partial p}{\partial r} = 0$

[a)]All expressions for $\overrightarrow{\Gamma_e}$ and $\overrightarrow{\Gamma_\varepsilon}$ denote BCs in the PS model only. [b)]$\psi \equiv n_{s\neq e,Ar}, T_e, T_h$. [c)]$\Phi$ is the gas flow rate and R_0 is the discharge tube radius; $u_r = 0$.

$$-\lambda_e \frac{\partial T_e}{\partial r}|_{R_0} = -k_B T_e(R_0)\left[2+\frac{1}{2}\ln\left(\frac{m_i}{m_e}\right)\right] D_A \frac{\partial n_e}{\partial r}|_{R_0}, \quad (39)$$

provided that there is no gas flow perpendicular to the wall. Applying $n_e = n_i$ at the plasma bulk-sheath boundary layer and Equation (36), the BC for the electron temperature becomes

$$-\lambda_e(R_0)\frac{\partial T_e}{\partial r}|_{R_0} = k_B T_e(R_0) n_i(R_0) v_{Bohm}\left[2+\frac{1}{2}\ln\left(\frac{m_i}{m_e}\right)\right]. \quad (40)$$

The sheath in the QN model is assumed to be infinitely thin and hence the BC for the electron temperature derived at the plasma bulk-sheath boundary layer can be applied as the corresponding BC at the wall for the electron energy balance equation in the QN model, i.e., Equation (22) solved with respect to T_e.

The expression for the Bohm velocity and the BC for the electron temperature derived above are valid when there is one type of positive ions. In the Ar plasma under study we may neglect the Ar_2^+ ions, since their density is 3 orders of magnitude lower than the density of the main Ar^+ ions (see below in Section Results and Discussion). If there is more than one type of positive ion, it is assumed that each type of ion satisfies the Bohm criterion[54] and an effective ion mass can be introduced based on the different type of ions and corresponding densities.

The BC for the heavy particle flux at the tube wall in the PS model is calculated from[64]

$$\Gamma_s(R_0) = \frac{\gamma}{(1-\gamma/2)}\frac{1}{4} n_s(R_0)\sqrt{\frac{8k_B T_h(R_0)}{\pi m_s}} + Z_s n_s \mu_s E_r H(E_r), \quad (41)$$

where γ is the sticking coefficient, equal to 1 for each type s of heavy particles. The second term is different from 0 only for the ions: Z_s is the charge of the corresponding ion, $H(E_r)$ is the Heaviside function (0 if Er is negative, 1 otherwise). The expression $\frac{1}{(1-\gamma/2)}$ is the Motz-Wise correction and we have found that it has a negligible effect for the conditions under study.

3.4. Validation of the Assumptions in the QN Model

In the QN model the time-derivative of the variables is neglected. This simplification is valid when the characteristic time of variation in plasma parameters greatly exceeds the time between collisions.[70] Since only the electrons can respond quickly to any perturbation of the quasi-neutrality or to a time varying electric field, we compare the electron, that is, plasma, frequency with the average electron-heavy particle collision frequency. The electron plasma angular frequency is given by $\omega_p[\mathrm{rad\,s^{-1}}] = \sqrt{\frac{e^2 n_e}{m_e \varepsilon_0}} = 56.4\sqrt{n_e[\mathrm{m^{-3}}]}$.[66] The electron density is in the order of 10^{19}–$10^{20}\,\mathrm{m^{-3}}$, and hence the plasma frequency $= \omega_p/2\pi$ is calculated to be in the range $2.8\text{–}9\times10^{10}\,\mathrm{s^{-1}}$, which is almost 2 orders of magnitude higher than the average total electron—Ar collision frequency $\bar{\nu}_{eAr}$, calculated to be in the range $2\text{–}20\times10^{8}\,\mathrm{s^{-1}}$. The latter is calculated from $\bar{\nu}_{eAr} = n_{Ar}\bar{\sigma}_{eAr}v_{e,th}$ taking the following values: the Ar density is 2.65×10^{22} and $2.65\times10^{23}\,\mathrm{m^{-3}}$ when the pressure is 100 and 1000 Pa, respectively. The electron thermal velocity $v_{e,th}$ is calculated by $v_{e,th}[\mathrm{ms^{-1}}] = \sqrt{\frac{8k_B T_e}{\pi m_e}} = 6.7x10^5\sqrt{T_e[\mathrm{eV}]}$, setting T_e to 2 and 1 eV at a pressure of 100 and 1000 Pa, respectively (see below for the simulation results and experimental measurements of T_e). The average total electron—Ar cross-section $\bar{\sigma}_{eAr}$ is in the order of $10^{-20}\,\mathrm{m^2}$. Therefore, in the pressure range under study this assumption is valid.

It is important to calculate also the electron mean free path, which is expressed by $v_{e,th}/\bar{\nu}_{eAr}$.[66] Applying the values above, the electron mean free path is calculated to be 0.335 and 4.5 mm at pressures of 1000 and 100 Pa, respectively.

Next, the plasma is considered quasi-neutral in the complete volume and therefore, sheaths are infinitely thin. The typical values of the electron temperature and density are 1 eV and $10^{20}\,\mathrm{m^{-3}}$, respectively, at the conditions under study. Hence, the Debye length $\lambda_D = \sqrt{\frac{\varepsilon_0 k_B T_e}{n_e e^2}}$ is 7.5×10^{-4} mm. The sheath width is in the order of λ_D,[71] and hence it can be indeed neglected in comparison with the plasma tube radius of 7 mm.

4. Plasma Diagnostics

In this work the OES measurements have been performed in the direction perpendicular to the discharge axis, collecting the light from a particular volume of interest using an Andor iStarDH740-18F-03 ICCD camera (see Figure 1). Figure 5a shows the emission spectra of Ar acquired in the wavelength range of 250–850 nm. As expected for typical Ar plasmas, the most intense emission lines correspond to the transition from the $4p \rightarrow 4s$ (or in Paschen notation: $2p \rightarrow 1s$) levels producing the emission peaks in the 660–1150 nm range. We can also observe the $5p \rightarrow 4s$ (or in Paschen notation: $3p \rightarrow 1s$) transitions emitted in the wavelength range $400 < \lambda\ (\mathrm{nm}) < 470$. Below the Paschen notation is used since it is more convenient in notation of the detected emission lines.

Plasma Process Polym 2017, 14, 1600185

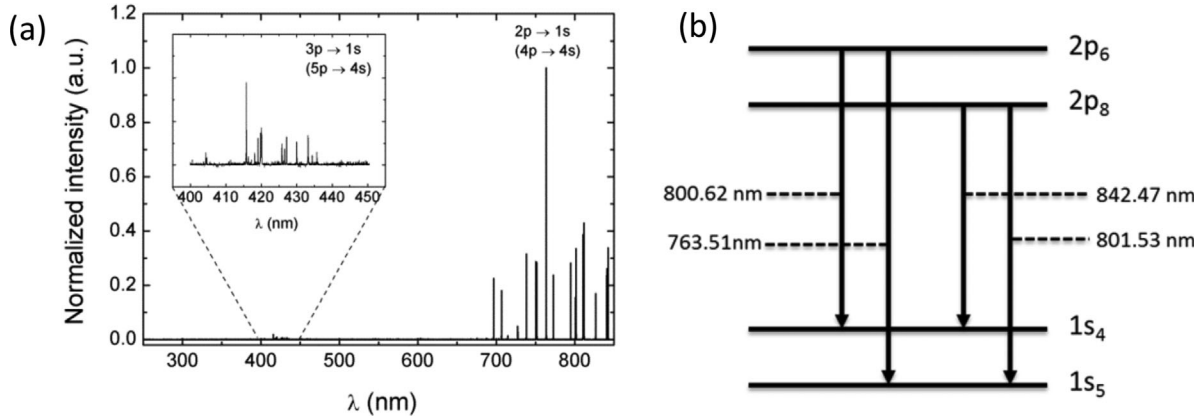

Figure 5. Emission spectrum from a pure Ar microwave surfaguide discharge (a). Inlet: Zoom of the $3p \rightarrow 1s$ (Paschen notation) emissions. An example of combining optical transitions $2p_y \rightarrow 1s_x$ ($4p \rightarrow 4s$) for the calculation of the Ar($1s_x$) densities (b).

The absolute population of the different atomic levels in the 1s group (formed by two metastable $1s_5$ and $1s_3$ and two resonant levels $1s_2$ and $1s_4$) was determined using so-called *passive spectroscopy*, based on the study of the self-absorption of photons generated in $2p \rightarrow 1s$ transitions. The self-absorption method has been extensively studied[76,77] and widely used in various spectroscopic measurements.[78–80] This method is suitable for absolute density measurements if the population of the lower state of a particular optical transition is high enough to provide a traceable optical thickness. In this case, the reabsorption of emission lines is taken into account via the concept of an escape factor,[79] which turns the emission transitions dependent on the metastable and resonant absolute population. This allows building a system of equations by combining line ratios between the intensities of two emission lines produced by de-excitation to two 1*s* levels from two higher 2*p* excited levels (see Figure 5b for a typical case). If one repeats this method for another pair of levels and pair of lines, all 1s populations can be determined.[59] Further details on evaluating the excited state densities, and the electron density and temperature based on the emission spectra are given in ref.[59]

The relative error of T_e has been estimated based on the so-called error propagation formulas[81] as a function of the relative errors of the line intensity ratio (δR) and normalized metastable state density ($\delta N(1s_5)$). Based on the top estimations for $\delta N(1s_5)$ and for δR (assuming typical ICCD emission line measured error $\sim$ 10%), the final value for δT_e estimated in our case is about 5%. The relative error of n_e is estimated similar to the relative error of T_e and is found to be also about 5%. The error of the Ar(4*s*) density is estimated based on the average of different experimental measurements which is in the range of 5–15%.

To estimate the gas temperature in an Ar plasma, the rotational temperature derived from the first positive system (FPS) of N_2 (via 5% N_2 admixture to the discharge) was utilized.[60]

The plasma emission in the OES measurements is collected by an optical fiber covering a cylindrical plasma volume with a height of 1 cm. The fiber is positioned at 4 cm above the waveguide gap. In order to compare the plasma characteristics calculated by the models with the experimentally measured values, the simulated plasma characteristics are averaged radially in a cylinder with height 1 cm at the same position in the simulation domain, that is, at 26 cm below the inlet (see Figure 2).

5. Results and Discussion

5.1. Comparison of the Plasma Characteristics, Calculated by the QN and PS Models

The output of the models gives information on the spatial distribution of a number of characteristics, that is, the species density and temperature, electric and magnetic field intensity, deposited power density, electron-heavy particle collision frequency, particle diffusion and thermal conductivity coefficients, etc. The following operating conditions are used as input: applied power of 100 W, pressure 1000 Pa, and gas flow rate of 125 sccm. Figure 6 presents the calculated electron density n_e (a), electron temperature T_e (b), gas temperature T_g (c), and Ar_2^+ density (d), calculated by the QN model (left column) and by the PS model (right column). The main Ar^+ ion density has a similar profile and values as the electron density, and therefore is not presented. The same color legend is used in the presentation of the plasma characteristics, calculated by the two models, to allow an easy comparison.

The wave form in the profiles and the position of the local maxima can be explained as follows. Surface waves are obtained only as slow waves[3] and the wave phase velocity

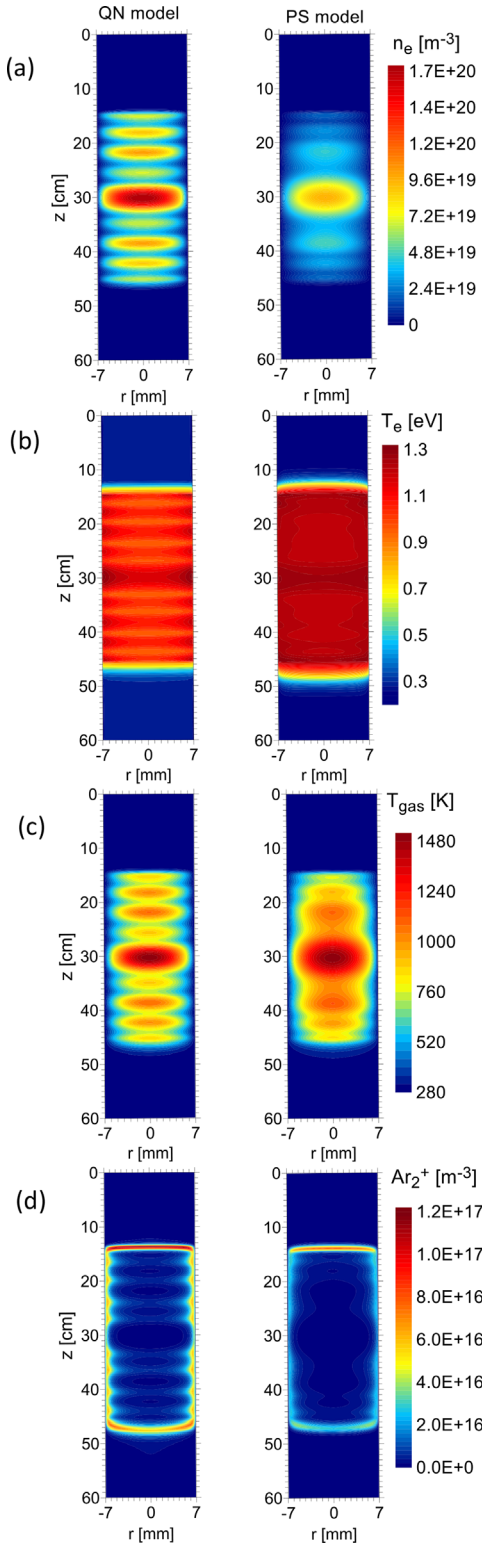

Figure 6. Electron density (a) and temperature (b), gas temperature (c) and Ar_2^+ density (d), calculated by the QN (left side) and PS (right side) models. The same color legend is used for both models to facilitate the comparison.

is 1.5×10^8 [$m\,s^{-1}$] (see Section Electromagnetic field equations, above). Thus the wavelength is calculated to be around 6 cm for the applied frequency of 2.45 GHz. The metal rings at the plasma tube ends (31 cm in length) confine the electromagnetic field and the surface waves can be reflected. In our experimental set up the tube length is shorter compared to the tube length of 60–80 cm used in the surfaguide experiments reported at pressures below 1000 Pa (cf. Refs.[26,37]). The local maximum values of the electron density (see Figure 4(a)) decrease twice from the center to the plasma tube end, which shows very weak wave damping because the tube length is comparatively short for the investigated pressure range. We found weak dissipation of the wave at the tube ends not only in the modeling results but also experimentally. Experimentally, we observed that the plasma column length is the same as the tube length for pressures between 80 and 3000 Pa, except for an applied power below 50 W at a pressure of 80 Pa in which case the plasma column contracted quickly with decreasing power and even the discharge extinguished below 40 W. Hence, we consider that standing waves are formed and local maxima along the tube length are formed at a distance close to a half wavelength (3 cm, see above). The local maximum values and the wavelength, and hence the distance between the maxima, along the tube, decrease away from the central position, where the wave is launched, due to plasma-wave interaction. In both models the local maximum values of the electron density (Figure 4(a)) have close to linear dependence with z, starting from the central position to the tube ends in agreement with previously reported 1D models in weakly collisional plasmas.[24–27] When the pressure increases, the electron-neutral collision frequency increases, which leads to significant contraction of the plasma column at atmospheric pressure.[40,41]

The maximum electron density, n_e, is calculated to be 1.1×10^{20} and 6×10^{19} m^{-3} in the QN model and PS model, respectively. Both values are radially averaged in front of the waveguide gap. The electron density decreases in the radial direction, away from the center, and its profile has Bessel-type form of the first kind, in agreement with the radial profile found analytically as a solution of the electron density balance equation.[33] Although the models operate with the same basic input, such as the Ar chemistry and reaction rate coefficients (see the Supporting Information), the heat capacity at constant pressure or constant volume and the viscosity of Ar, and the Ar^+ diffusion coefficient, the different diffusion regimes, and hence the different BCs for the particle fluxes at the wall might explain the difference in the electron density values calculated by the two models. We observe that the profiles calculated by the QN model are more pronounced, which is due possibly to the different mesh and numerical approach for solving the equations in the two modeling frameworks. In the QN model a

structured mesh in the form of an ordered rectangular grid is used. The computational domain consists of 482 cells in the axial direction and 202 in the radial direction. In axial direction the cells are stretched towards the ends, so that the size gradually changes from 2.073 mm at the edges to 0.833 mm in the center. In the radial direction the cells are stretched beyond a radius of 7 mm, so that up to 7 mm their size is 0.167 mm and for higher radii the size gradually increases up to a size of 0.635 mm. The portion of the computational domain occupied by the plasma is therefore 42 cells in radial direction over the entire length. In the PS model, a non-uniform triangular grid in the plasma volume and a finer non-uniform quadrilateral grid next to the plasma tube wall is constructed, based on algorithms described in the manual of COMSOL.[64] The number of the triangular cells in the computational domein is 25,810 and the number of the quadrilateral cells is 7428. Regarding the numerical algorithms used for solving the equations, information can be found in the documentation of PLASIMO[63] and COMSOL.[64]

The radially averaged T_e (Figure 4(b)) in the discharge center is calculated to be 1.1 and 1.27 eV by the QN and PS models, respectively. The profile of T_e does not change considerably in the volume, and is in the order of 1 eV. Therefore, the temperature gradients in the plasma can be neglected compared to the density gradients (see for instance the profile of the electron density presented in Figure 4(a)).[70] The difference in the values of T_e calculated by both models is comparatively small (in the order of 15%). A reason might be neglecting the additional terms in the electron heat flux vector in the QN model, which requires further investigation, as discussed in Section Specific Energy Balance Equations.

The spatial profile of T_g is similar to the profile of the electron density since the elastic collisions are the main gas heating mechanism. There is a good agreement both in the profile and the values of the gas temperature calculated by the two models. Still, we consider to improve the heavy particle energy balance equations by the addition of the term neglected in the heat flux vector when the gas flow is not 0 (the last term in Equation (32)). Only a few models consider these terms till now, however, they are developed for localized MW plasma created in resonant cavity reactors[54,82] and therefore, a comparison is difficult to make.

The density of the molecular ions Ar_2^+ exhibits maximum values close to the tube wall and at the plasma column ends, that is, where T_g is low. Analysis of the reaction rates for formation and loss of the molecular ion shows that high T_g reduces the population of the molecular ion.[42] The maximum calculated value is 1.2×10^{17} and $0.8 \times 10^{17}\,m^{-3}$ in the QN and PS model, respectively.

The maximum values of the Ar(4*s*) density (not shown here) calculated by the two models in the order of $1–2 \times 10^{18}\,m^{-3}$ are found at the plasma column ends, which is in agreement with experimental measurements along the *z*-axis in surfatron sustained Ar discharges.[49,52] The radially averaged density in the discharge center is in the order of $5–6 \times 10^{17}\,m^{-3}$. The density of Ar(4p), again radially averaged in the discharge center, is $4 \times 10^{17}\,m^{-3}$ and $2 \times 10^{17}\,m^{-3}$ in the QN and PS model, respectively. Due to the higher electron density calculated in the QN model, all other species have up to twice as high values compared to the corresponding densities calculated in the PS model.

Figure 7 presents the electron density (a) and temperature (b) and the gas temperature (c) calculated by both models for an applied power of 50–200 W at a pressure of 1000 Pa and flow rate of 125 sccm. Figure 7(a) shows the linear dependence of the electron density on applied power, in agreement with theoretical and experimental studies previously reported.[1–3,42]

Experimental measurements for similar pressure (1000 Pa) and similar quartz tube radius are scarce in literature. A similar surfaguide reactor sustains Ar plasma in a quartz tube with a radius of 7.5 mm.[26] The electron density is measured at a pressure of 133 Pa (1 Torr). Based on

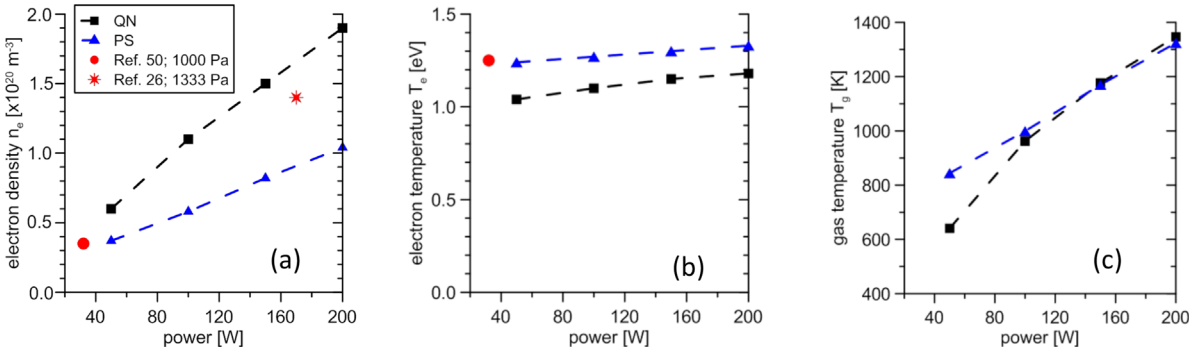

Figure 7. Radially averaged electron density (a) and temperature (b), and gas temperature (c) calculated by the QN and PS models as a function of the applied power at 1000 Pa and 125 sccm. The legend in (a) also applies for (b) and (c). The measurements available in the literature at 1333 Pa in surfaguide[26] and at 1000 Pa in surfatron[50] Ar discharges are shown.

the experimental measurements, laws of similarity have been developed and used to calculate the electron density at different operating conditions.[26] For example, n_e in front of the waveguide gap was calculated to be 1.4×10^{20} m^{-3} at a pressure of 1333 Pa and applied power of 170 W.[26] The other relevant reference we have found considers measurements of the electron density in a surfatron Ar discharge sustained in a quartz tube with a radius of 3 mm.[50] The electron density at the position where the wave is launched is measured to be around 4×10^{19} m^{-3} at a pressure of 1000 Pa and applied power of 32 W.[50] The measured T_e at the same operating condition is 1.3 eV. The experimental measurements listed above are shown in Figure 7(a) and (b).

We could not find simulation results or experimental measurements of the gas temperature in SW sustained Ar discharges at a pressure of 1000 Pa in the literature. We find, however, good agreement with measurements at lower pressure (see the next section).

The developed simulation models also have limitations. When the pressure decreases, the mean free path of the electrons increases and at 100 Pa, it is calculated to be 4.5 mm (see Section Validation of the assumptions in the QN model), which is comparable with the radius of the plasma tube (7 mm). The minimum pressures (independently of the applied power) at which the developed QN and PS models produce stable solutions are 200 and 600 Pa, respectively. The lower pressure limit for the QN model can be explained by the calculated higher electron density compared to the values calculated by the PS model. In both models at pressures below the critical value for each model, we observed that the charged particles are lost at the wall faster than their creation in the plasma bulk. We extend the pressure range by the experimental measurements done in the modeled set-up at lower pressure. The results are presented in the next section.

5.2. Pressure Range Extension by Experimental Measurements

The plasma characteristics were measured for a pressure range of 80–170 Pa, which corresponds to a flow rate range of 25–175 sccm, since a change in pressure is connected to a change of the flow rate at which the gas is supplied in the experimental set-up. The flow rate in the simulations is kept fixed at 125 sccm, or 2.08×10^{-6} m^3 s^{-1}, which is not a very large value at standard temperature and pressure. However, at a pressure of 200 Pa, it is 4.22×10^{-3} m^3.s^{-1}. Taking into account the plasma tube cross-section of 1.54×10^{-4} m^2 and a parabolic velocity profile, the maximum gas flow velocity is along the axis of symmetry and is calculated to be 14 m.s^{-1}. Therefore, neglecting the gas flow velocity will affect the plasma transport, especially for the heavy particles, in the axial direction. Indeed, we performed some simulations without gas flow, and the results show that the gas temperature in the discharge centre is calculated to be about 660 K, which is 25% higher compared to the results for a gas flow of 125 sccm (i.e., 530 K). At a pressure of 1000 Pa, the gas flow velocity is 3 m.s^{-1}. The difference in the gas temperature with or without gas flow is then less pronounced and is about 7%. The gas temperature without flow is calculated to be 1030 K, while it is 960 K at a flow rate of 125 sccm. We investigated the influence of the flow rate from 125 till 500 sccm and found that the plasma characteristics do not depend on the flow rate in the considered power regime, only the profile changes slightly in the direction of the flow. However, when we increase further the flow rate till 1000 sccm, and at a power of 500 W, we observe highly asymmetric profiles and extension of the plasma outside of the EM region in the direction of the flow,[21] which cannot be observed when the gas flow is 0. In the experiment in ref.[21] a catalytic reactor is placed 3 cm below the bottom EM confinement ring positioned at 45.5 cm. The simulation predicts a gas temperature in the order of 600–800 K in the catalytic reactor. The extension of the plasma is detected experimentally by measuring a high gas temperature of about 600 K in the catalytic reactor (note that the cooling system keeps the plasma tube wall temperature at 5 °C).[21] For a comparison, at a low flow rate used in the present work, the gas temperature measured and predicted by the simulations (see Figure 6(c)) at the same position ($z = 48.5$–50 cm) is close to room temperature.

Figure 8(a) presents the measured and simulated electron temperature as a function of pressure at an applied power of 100 W. The decrease of T_e with pressure is attributed to more frequent electron-neutral collisions when the pressure increases. The experimental data are fitted linearly and the fit is extrapolated to a pressure of 200 Pa, which corresponds to the first simulation point. The extrapolated value of 1.4 eV is in good agreement with the calculated value of 1.37 eV at 200 Pa by the QN model. The measurements in a surfatron sustained Ar discharge available in the literature show also a decrease of T_e with pressure[50] and are in good agreement with our simulation results, especially with the results from the PS model.

The radially averaged electron density at 4 cm above the wave launcher (or 26 cm along the z-axis) and in front of the wave launcher calculated by the QN and PS models are shown in Figures 8(b) and (c), respectively. The estimation of the electron density based on the OES measured plasma emission at 4 cm above the wave launcher is also shown in Figure 8(b). The calculated electron density at 200 Pa is about six times higher than the measured one at 170 Pa (see below in Table 2, which presents the experimental and simulation results at their pressure limits). The difference in the calculated and measured electron densities might be explained by the reaction rate coefficients used in the

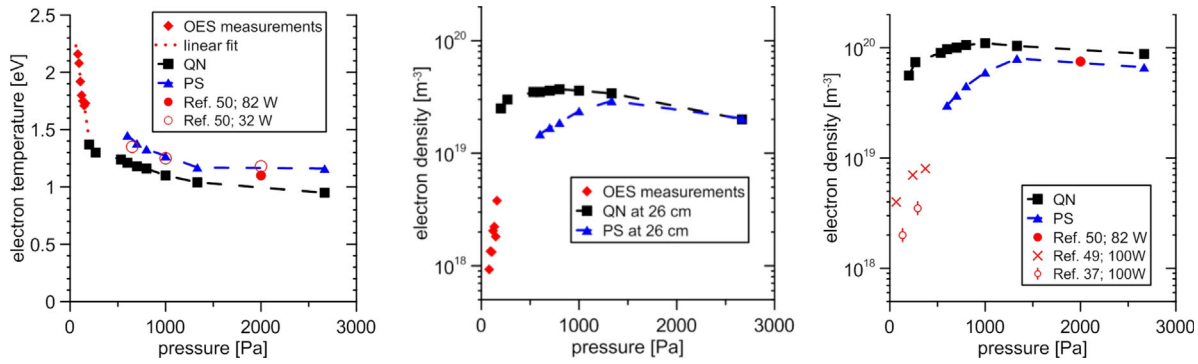

Figure 8. Comparison of electron temperature (a) and density (b and c), experimentally estimated based on OES measured plasma emission and calculated by the QN and PS models, as a function of pressure, for an applied power of 100W: (b) electron density at 4 cm above the waveguide gap, that is, at 26 cm along the *z*-axis; (c) electron density calculated in the discharge center, that is, at 30 cm along the *z*-axis. The measured electron temperature[50] and electron density[49,50] in front of the wave launcher in a surfatron Ar discharge are presented in (a) and (c), respectively. The measured electron density in the discharge center of a surfaguide Ar discharge[37] is presented in (c).

analysis of the optical emission spectra, considering each $1s_y$ level separately,[59] which are different from the reaction rate coefficient in the simulation, where a single lumped excitation level 4*s* is considered. The measured (see Table 2) n_e of 4×10^{18} m^{-3} (160 Pa, 100 W, 175 sccm) is in good agreement with the electron density of 2×10^{18} m^{-3} measured in a surfaguide Ar discharge at similar operating conditions (133 Pa, 100 W, 100 sccm).[37]

The calculated electron density in the discharge center is compared with measurements available in the literature in surfatron[49,50] and surfaguide[37] Ar discharges (see Figure 8c). Investigation of the electron density as a function of pressure by the QN and PS models shows that the electron density starts to decrease at a pressure above 1333 Pa. In that region, the volume recombination and the molecular assisted recombination start to play a role and therefore the charged particle density decreases, although the electron-Ar collision frequency increases with pressure. This observation is in agreement with the classification[3] according to the *pR* product (see the Introduction).

Table 2 presents the measured plasma characteristics and the calculated values by the QN model at 170 and 200 Pa, respectively. As explained above, the critical minimum pressure at which the PS model is reliable is 600 Pa, and therefore the calculated values of the PS model could not be compared with the experimental data, which explains why they are not included in Table 2. The simulated plasma characteristics are radially averaged in a cylindrical volume of 1 cm height, at 4 cm above the discharge center, where the optical fiber is positioned. Good agreement in T_e, T_g, and Ar(4*s*) density is observed. Our data for T_g are in good agreement also with the measured T_g of around 480 K in a surfaguide Ar discharge at similar operating conditions (133 Pa, 100 W, 100 sccm).[37]

Finally, we present the results for the plasma potential calculated in the PS model by solving Poisson's equation. When resolving the sheath region in the PS model, a special boundary rectangular mesh is used. At the boundary, the length of the cell in the *r*-direction is 0.01 mm and it is 0.5 mm in the *z*-direction. We observed no large variations of the calculated plasma potential when decreasing the mesh size. The equation is discretized linearly. The radial distribution of the plasma potential at $z = 0$ for a pressure range 600–2667 Pa is shown in Figure 9. The sheath width, defined as the distance from the wall where considerable deviation from quasineutrality is observed was found to be in the order of, or less than, 0.1 mm. The plasma potential and the sheath drop decrease from 15 to 13 V and from 12 to

Table 2. Plasma characteristics calculated by the QN model and measured by OES or FPS at 4 cm above the wave launcher.

	T_e [eV]	n_e[m^{-3}]	T_g [K]	Ar(4s) density [m^{-3}]
Modeling 200 Pa, 50 W	1.3	1.5×10^{19}	396	2.2×10^{17}
Experiment[a)] 170 Pa, 50 W	1.65	0.2×10^{19}	400 ± 90	2.8×10^{17}
Modeling 200 Pa, 100 W	1.37	2.5×10^{19}	463	2.3×10^{17}
Experiment 160 Pa, 100 W	1.7	0.4×10^{19}	450 ± 60	2.4×10^{17}

[a)]Incident power. The reflected power in the experiment has always a non-zero value, and for all cases it is measured to be in the range 3–6% from the incident power.

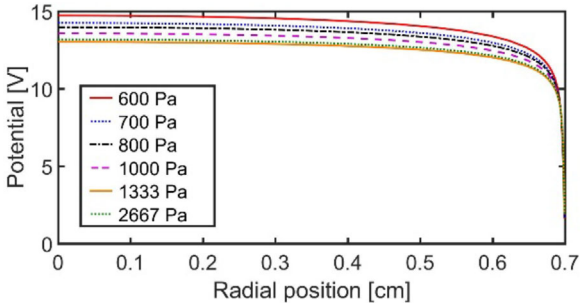

Figure 9. Plasma potential radial distribution at $z = 0$, calculated in the PS model for different pressures.

10 V, respectively, when the pressure increases from 600 to 1333 Pa. Both parameters almost do not change at 2667 Pa. The same behavior is observed in the electron temperature dependence on pressure (see Figure 8(a)). The sheath potential difference in ambipolar electric field approximation (QN model) is given by Equation (38). It is proportional to the electron temperature and is calculated to be 5–6 V for $T_e = 1.0$–1.2 eV in the QN model in the considered pressure range of 600–2667 Pa. Hence, in both models the potential drop across the sheath is proportional to the electron temperature.

6. Conclusion

We present and benchmark two 2D self-consistent models of a surface-wave sustained Ar discharge operating at intermediate pressure in the range of 200–2667 Pa, and extended down to 80 Pa by experimental data measured in the simulated set-up. The plasma is sustained by electromagnetic waves launched by a surfaguide reactor operating at 2.45 GHz in continuous regime. One of the models considers quasi-neutral plasma in the complete plasma region and neglects sheath formation (QN model) and the other model resolves the formation of the sheath (PS model). Both models solve the electromagnetic field equations describing the surface wave propagation along the plasma-dielectric border. The complete general set of fluid (transport) equations is presented in local and laboratory reference frames. The additional terms in the heat flux vector and hence in the energy balance equations due to the transformation from a local to a laboratory reference frame are derived and discussed. The specific density and energy balance equations along with the corresponding BCs are developed and compared for the two models. The transport coefficients used in the models are given. The gas flow is taken into account through solving the plasma continuity and momentum equations.

The models are benchmarked at a pressure of 1000 Pa. The similarities and differences are discussed based on the set of equations and corresponding BCs solved in each model, the applied transport coefficients and diffusion approximations. We found good agreement in the calculated power deposition density and electric field, and in general in all plasma characteristics. The influence of power and pressure on the plasma characteristics is presented and discussed. Both simulation models show that the electron temperature decreases with pressure till 1333 Pa and is more or less constant close to 1 eV when the pressure is increased further. The electron density increases till 1333 Pa, and then starts to decrease due to loss of charged particles via volume and molecular-assisted recombination. The change in the plasma behavior is in agreement with a previously developed classification[3] based on the pressure-radius pR product. The electron density and gas temperature have a dependence on the applied power close to linear.

The pressure limitation of the models is clarified. Therefore, the modeling results were extended in the pressure range by experimental measurements carried out in the modeled set-up. Comparison with experimentally measured plasma characteristics available from literature for similar operating conditions is also shown and discussed. A good agreement is found, taking into account a number of different operating conditions and reactors.

In conclusion, both diffusion approximations can be applied successfully to simulate the SW sustained plasmas at the intermediate pressure range. The modeled Ar plasma characteristics are benchmarked with previously developed analytical solutions or parametrizations, as well as with experimental measurements available in literature. Hence, the developed 2D models can be adapted in future to simulate complex chemical plasmas, which are of interest for environmental or industrial applications.

Acknowledgements: This research is carried out in the framework of the network on Physical Chemistry of Plasma Surface Interactions – Interuniversity Attraction Poles phase VII project (http://psi-iap7.ulb.ac.be/), supported by BELSPO. N. Britun is a post-doctoral researcher of the FNRS, Belgium. A. Berthelot's research was supported by the European Marie Curie RAPID project, which has received funding from the European Union's Seventh Framework Programme for research, technological development and demonstration under grant agreement no 606889.

Supporting Information is available from the Wiley Online Library or from the author.

Appendix

Transport Equations in Local and Laboratory Reference Frames

Information for the macroscopic variables can be derived from the BE, Equation (12) from the main paper, without solving it. A macroscopic variable $\chi(\vec{r},\vec{v},t)$ is related to the moment of the distribution function as shown by Equation (11). The transport equation of that variable can be obtained by taking the corresponding moment of the BE, which means multiplying the BE by χ and integrating over all the velocity space. When χ is dependent only on position $\vec{r}$, and time t, the transport equation is given by[69]

$$\frac{\partial}{\partial t}\left(n_\alpha\langle\chi\rangle_\alpha\right)+\nabla.\left(n_\alpha\langle\chi\vec{v}\rangle_\alpha\right) - n_\alpha\left\langle\frac{\vec{F}}{m_\alpha}.\nabla_v\chi\right\rangle_\alpha=\int_v\chi\left(\frac{\delta f_\alpha}{\delta t}\right)_{coll}d^3v. \quad (A1)$$

The specific density, momentum, and energy balance equations are derived from the zero-th, (i.e., $\chi\equiv 1$), first $(\chi\equiv m_\alpha\vec{v})$,and second $\left(\chi\equiv\frac{m_\alpha v^2}{2}\right)$ moments of the Boltzmann equation, respectively. Combinations of these equations form the continuity equation and the momentum equation for the plasma as a whole.

The specific density equation is obtained from Equation (A1) by setting $\chi\equiv 1$ and applying Equation (16) from the main paper.[69] In addition, the particle flux defined as $\vec{\Gamma}_\alpha=n_\alpha\vec{u}_\alpha=n_\alpha(\vec{u}+\vec{w}_\alpha)$, is a sum of two components: the particle flux due to the collective motion of all particles $n_\alpha\vec{u}$ and the diffusion particle flux $\vec{\Gamma}_{\alpha,dif}=n_\alpha\vec{w}_\alpha$. Hence, the specific density equation in particle velocity representations with respect to $\vec{u}_\alpha$ or to $\vec{u}$ is given by

$$\frac{\partial n_\alpha}{\partial t}+\vec{\nabla}.(n_\alpha\vec{u}_\alpha)=\left[\frac{\delta(n_\alpha)}{\delta t}\right]_{coll}, \quad (A2)$$

$$\frac{\partial n_\alpha}{\partial t}+\vec{\nabla}.(n_\alpha\vec{u})+\vec{\nabla}.\vec{\Gamma}_{\alpha,dif}=\left[\frac{\delta(n_\alpha)}{\delta t}\right]_{coll}. \quad (A3)$$

The continuity equation is obtained by multiplying Equation (A2) or (A3) by m_α, and summing over all species. Having the total mass density ρ_m, the average plasma velocity expressed by Equation (13) from the main paper, taking into account Equation (17) and the fact that the collision term vanishes when summing over all species, as a consequence of the total mass conservation of the system, we receive

$$\frac{\partial\rho_m}{\partial t}+\vec{\nabla}.(\rho_m\vec{u})=0. \quad (A4)$$

The specific momentum equation is obtained from Equation (A1) by setting $\chi\equiv m_\alpha\vec{v}$. The formulation with respect to the particle velocity $\vec{v}$ presentation relative to $\vec{u}_\alpha$ is[69]

$$\frac{\partial}{\partial t}(\rho_\alpha\vec{u}_\alpha)+\vec{\nabla}.(\rho_\alpha\vec{u}_\alpha\vec{u}_\alpha) + \vec{\nabla}.\bar{\bar{\mathrm{P}}}_\alpha-\mathrm{n}_\alpha<\vec{F}>_\alpha=\vec{\mathrm{A}}_\alpha, \quad (A5)$$

where $\vec{A}_\alpha$ is the exchange of momentum between different species by means of collisions, $\bar{\bar{\mathrm{P}}}_\alpha=\rho_\alpha\vec{c}_\alpha\vec{c}_\alpha$ is the kinetic pressure tensor and is expressed further by the scalar pressure p_α and the viscosity tensor $\bar{\bar{\tau}}_\alpha$ (see Equation (A14) below). The external force $\vec{F}$ in plasma is electromagnetic in nature and is given by the Lorentz force: $\vec{F}=Z_\alpha e\left(\vec{E}+\vec{v}\times\vec{B}\right)$, where Z_α is the charge number of the species α and e is the elementary charge; $\vec{B}=\mu_0\vec{H}$ is the magnetic induction vector. The gravitational force is neglected. Hence, for the charged particles the averaged external force is $\left\langle\vec{F}\right\rangle_\alpha=Z_\alpha e\left(\vec{E}+\vec{u}_\alpha\times\vec{B}\right)$, and for the neutral particles the external force is 0. Equation (A5) in two velocity presentations is

$$\frac{\partial}{\partial t}(\rho_\alpha\vec{u}_\alpha)+\vec{\nabla}.(\rho_\alpha\vec{u}_\alpha\vec{u}_\alpha)+\nabla p_\alpha + \vec{\nabla}.\bar{\bar{\tau}}_\alpha-n_\alpha Z_\alpha e\left(\vec{E}+\vec{u}_\alpha\times\vec{B}\right)=m_\alpha\left[\frac{\delta(n_\alpha\vec{u}_\alpha)}{\delta t}\right]_{coll} \quad (A6)$$

$$\frac{\partial}{\partial t}(\rho_\alpha\vec{w}_\alpha)+\vec{\nabla}.(\rho_\alpha\vec{u}\vec{w}_\alpha)+\rho_\alpha(\vec{w}_\alpha.\vec{\nabla})\vec{u}+\rho_\alpha\frac{D\vec{u}}{Dt}+\nabla p'_\alpha+\vec{\nabla}.\bar{\bar{\tau}}'_\alpha$$

$$-n_\alpha Z_\alpha e(\overline{E'}+\vec{w}_\alpha\times\vec{B})==m_\alpha\left[\frac{\delta(n_\alpha\vec{w}_\alpha)}{\delta t}\right]_{coll} \quad (A7)$$

The expressions for kinetic pressure tensor $P^{=\prime}{}_a$, the scalar pressure p'_a, viscosity tensor $=\tau_a'$ and electric field $\overline{E'}$ in the particle velocity representation relative to $\vec{u}$ are given below in Section Definition of quantities in two velocity representations.[69]

In absence of an external magnetic field, neglecting viscosity and time dependence of $\vec{u}$, applying the relations (A29), Equation (A7) is transformed to

$$\frac{\partial}{\partial t}(\rho_\alpha\vec{w}_\alpha)+\vec{\nabla}.(\rho_\alpha\vec{u}\vec{w}_\alpha)+\rho_\alpha(\vec{w}_\alpha.\vec{\nabla})\vec{u}+\nabla p_\alpha$$

$$-\mathrm{n}_\alpha Z_\alpha e\vec{E}=m_\alpha\left[\frac{\delta(n_\alpha\vec{w}_\alpha)}{\delta t}\right]_{coll}. \quad (A7a)$$

The momentum balance equation for the plasma or the equation of motion for the plasma as a whole is obtained by summing Equation (A.6) or (A.7) over all species in the plasma.[69] Taking into account that the exchange of momentum due to collisions for the plasma as a whole is 0, and introducing the total electric charge density per unit volume $\rho = \sum_{\alpha} n_{\alpha} Z_{\alpha} e$, we obtain[69]

$$\frac{\partial}{\partial t}(\rho_m \vec{u}) + \vec{\nabla} \cdot (\rho_m \vec{u}\vec{u}) + \vec{\nabla} \cdot \mathrm{P}^{=} - \left(\rho \vec{E} + \vec{J} \times \vec{B}\right) = 0, \quad \text{(A8)}$$

where the total kinetic pressure tensor $\overline{\overline{\mathrm{P}}}$ and the total electric current density $\vec{J}$ are developed in Section Definition of quantities in two velocity representations.[69] If the plasma is neutral, that is, ρ is 0, no external magnetic field is applied and using Equation (A30), Equation (A8) is transformed to

$$\frac{\partial}{\partial t}(\rho_m \vec{u}) + \vec{\nabla}.(\rho_m \vec{u}\vec{u}) + \nabla p + \vec{\nabla}.\overline{\overline{\tau}} = 0. \quad \text{(A9)}$$

Equation (A4) and (A9) are known as Navier-Stokes equations.

The *specific energy balance* is obtained from Equation (A1) by setting $\chi \equiv \frac{m_\alpha v^2}{2}$. In the presentation relative to $\vec{u}_a$: $v^2 = u_\alpha^2 + \langle c_\alpha^2 \rangle$, and the total average particle energy is a sum of the kinetic energy of directed motion and kinetic energy of random, thermal, motion

$$\chi \equiv K_{u_\alpha} + \varepsilon_\alpha = \frac{m_\alpha u_\alpha^2}{2} + \frac{m_\alpha \langle c_\alpha^2 \rangle}{2}. \quad \text{(A10)}$$

For an isotropic distribution of the random velocity

$$\varepsilon_\alpha = \frac{m_\alpha \langle c_\alpha^2 \rangle}{2} = \frac{3}{2} k_B T_\alpha. \quad \text{(A11)}$$

Introducing the heat flux vector (which is the random flux of the thermal energy) $\vec{q}_\alpha = \frac{1}{2}\rho_\alpha \langle c_\alpha^2 \vec{c}_\alpha \rangle$, and applying Equation (A2) and (A6), the specific energy balance equation in velocity presentation relative to $\vec{u}_\alpha$ is

$$\frac{\partial}{\partial t}(n_\alpha \varepsilon_\alpha) + \vec{\nabla}.(n_\alpha \varepsilon_\alpha \vec{u}_\alpha) + (\overline{\overline{\mathrm{P}}}_\alpha.\vec{\nabla}).\vec{u}_\alpha + \vec{\nabla}.\vec{q}_\alpha = \left[\frac{\delta(n_\alpha \varepsilon_\alpha)}{\delta t}\right]_{coll}. \quad \text{(A12)}$$

A derivation of the equation can be found in ref.[69] Note that the external force term vanishes in that velocity presentation.

The specific energy balance equation can be written with particle velocity representation with respect to the average plasma velocity.[65,69] The derivation is too tedious to be shown here. It is based on the specific continuity equation (A3), the specific momentum transfer equation (A7), and the transformations (A18)–(A28). The final general form is[65,69]

$$\frac{\partial}{\partial t}(n_\alpha \varepsilon'_a) + \vec{\nabla}.(n_\alpha \varepsilon'_\alpha \vec{u}) + \rho_\alpha \vec{w}_\alpha \frac{D\vec{u}}{Dt} + (\overline{\overline{P}}'_\alpha.\vec{\nabla}).\vec{u} + \vec{\nabla}.\vec{q}'_\alpha - n_\alpha Z_\alpha e \vec{w}_\alpha.\vec{E}' = \left[\frac{\delta(n_\alpha \varepsilon'_\alpha)}{\delta t}\right]_{coll} \quad \text{(A13)}$$

The term in the right-hand side of Equation (A12) and (A13) represents the rate of change in the thermal energy density due to collisions and radiation.

In plasma, the viscosity effect in energy transport can usually be neglected.[69,70] In both models presented here we neglect the viscosity terms in the specific energy balance equations. Applying Equation (A14) for the kinetic pressure tensor, and the relations (A29) and (A32), neglecting the time dependence of $\vec{u}$, and in absence of an external magnetic field (see (A27)), Equation (A13) becomes

$$\frac{\partial}{\partial t}(n_\alpha \varepsilon_\alpha) + \vec{\nabla}.(n_\alpha \varepsilon_\alpha \vec{u}) + p_\alpha \vec{\nabla}.\vec{u} + \vec{\nabla}.(\vec{q}_\alpha + p_\alpha \vec{w}_\alpha + n_\alpha \varepsilon_\alpha \vec{w}_\alpha) - n_\alpha Z_\alpha e \vec{w}_\alpha.\vec{E} = \left[\frac{\delta(n_\alpha \varepsilon_\alpha)}{\delta t}\right]_{coll}. \quad \text{(A13a)}$$

The last term in the left-hand side is the Ohmic (Joule) heating, $Q_{ohm} = -n_e e \vec{w}_e.\vec{E} = \overline{\vec{J}}.\vec{E}$, when α denotes electrons; and it is 0 when α denotes ions since the ion current is neglected (see also Equation (A28), showing that $\overline{\vec{J}}$ and $\vec{J}$ are equivalent when the plasma is neutral).

Kinetic pressure tensor

The kinetic pressure tensor can be presented as a sum of the scalar pressure of particles type α, p_a, and the viscous stress tensor, $\overline{\overline{\tau}}_\alpha$[69–71]

$$P_{\alpha ij} = p_\alpha \delta_{ij} + \tau_{\alpha ij}. \quad \text{(A14)}$$

Here δij is the Kroenecker delta defined as $\delta_{ij} = 1$ for $i = j$, $\delta_{ij} = 0$ for $i \neq j$, for $i, j = 1, 3$. The scalar pressure p_a is defined as one-third the trace of the pressure tensor[69]

$$p_\alpha = \frac{1}{3}\sum\nolimits_{i=1,3} P_{\alpha ii} = \frac{1}{3}\rho_\alpha \langle c_\alpha^2 \rangle. \quad \text{(A15)}$$

According to the thermodynamic definition of the absolute temperature T_α, there is a mean thermal energy associated with each translational degree of freedom $(i = 1, 3)$: $\frac{1}{2}k_B T_{\alpha i} = \frac{1}{2} m_\alpha < c_{\alpha i}^2 >$. When the distribution of the random velocity is isotropic $c_{\alpha i}^2 = c_\alpha^2/3$ (which is the case of the Maxwell-Boltzmann distribution) the scalar pressure is given by the equation of state of an ideal gas[69]

$$p_\alpha = \rho_\alpha < c_{\alpha i}^2 >= n_\alpha k_B T_\alpha. \quad \text{(A16)}$$

Plasma Process Polym **2017,** *14*, 1600185

The viscous-stress tensor elements are defined as[69,70]

$$\tau_{\alpha ij} = \rho_\alpha < \vec{c}_{\alpha i}\vec{c}_{\alpha j} - \frac{1}{3}c_\alpha^2\delta_{ij} > . \quad \text{(A17)}$$

When the viscosity effect is relatively unimportant (typically this is valid for the electrons), the non-diagonal elements of $P_{\alpha ij}$ can be neglected. Hence, the force per unit volume inside the plasma, $-\vec{\nabla}.\overline{\overline{P}}_\alpha$, is reduced to the negative gradient of the scalar pressure: $-\vec{\nabla}.\overline{\overline{P}}_\alpha = -\nabla p_\alpha$.

Definition of quantities in two velocity representations[69]

1) Relative to the average particle velocity: $\vec{v} = \vec{u}_\alpha + \vec{c}_\alpha$, that is, in a reference frame moving with the plasma flow velocity, or in a laboratory reference frame if the plasma flow velocity is 0.
2) Relative to the average plasma velocity: $\vec{v} = \vec{u} + \vec{c}_{\alpha 0}$, that is, in a laboratory reference frame. The corresponding quantities are denoted with a superscript′

$$< \vec{v} >_\alpha = \vec{u}_\alpha = \vec{u} + \vec{w}_\alpha, \quad \text{(A18a)}$$

$$< \vec{c}_\alpha >_\alpha = 0; \quad < \vec{u}_\alpha >_\alpha = \vec{u}_\alpha; \quad < \vec{c}_{\alpha 0} >_\alpha = \vec{w}_\alpha; \quad < \vec{u} >_\alpha = \vec{u} \quad \text{(A18b)}$$

$$\vec{c}_{\alpha 0} = \vec{c}_\alpha + \vec{w}_\alpha, \quad \text{(A18c)}$$

$$< v^2 >_\alpha = u_\alpha^2 + < c_\alpha^2 >_\alpha, \quad \text{(A18d)}$$

$$< v^2 >_\alpha = u^2 + < c_{\alpha 0}^2 >_\alpha + 2\vec{u}.\vec{w}_\alpha. \quad \text{(A18e)}$$

Below the subscript α in the expression for average values is omitted.

$$\textit{Particle pressure tensor}: \quad \overline{\overline{P}}_\alpha = \rho_\alpha \langle \vec{c}_\alpha \vec{c}_\alpha \rangle,$$
$$\overline{\overline{P}}'_\alpha = \rho_\alpha \langle \vec{c}_{\alpha 0} \vec{c}_{\alpha 0} \rangle.$$

Applying that

$$\langle \vec{c}_{\alpha 0}\vec{c}_{\alpha 0} \rangle = \langle (\vec{c}_\alpha + \vec{w}_\alpha)(\vec{c}_\alpha + \vec{w}_\alpha) \rangle = \langle \vec{c}_\alpha \vec{c}_\alpha \rangle + 2\vec{w}_\alpha \langle \vec{c}_\alpha \rangle + \langle \vec{w}_\alpha \vec{w}_\alpha \rangle = \langle \vec{c}_\alpha \vec{c}_\alpha \rangle + \vec{w}_\alpha \vec{w}_\alpha,$$

the relationship between the two presentations of the kinetic pressure tensor is:

$$\overline{\overline{P}}'_\alpha = \overline{\overline{P}}_\alpha + \rho_\alpha \vec{w}_\alpha \vec{w}_\alpha. \quad \text{(A19)}$$

Partial scalar pressure

$$p'_\alpha = \frac{1}{3}\sum_{i=1,3} P'_{\alpha ii} = \frac{1}{3}\rho_\alpha \langle c_{\alpha 0}^2 \rangle = p_\alpha + \frac{1}{3}\rho_\alpha w_\alpha^2. \quad \text{(A20)}$$

$\overline{\overline{P}}'_\alpha$ can be written in the form of Equation (A14), that is, a sum of the scalar pressure, p'_α, and viscosity tensor, $\overline{\overline{\tau}}'_\alpha$, relative to the plasma flow velocity

$$\overline{\overline{P}}'_\alpha = p'_\alpha \overline{\overline{I}} + \overline{\overline{\tau}}'_\alpha. \quad \text{(A21)}$$

The relationship between $\overline{\overline{\tau}}_\alpha$ and $\overline{\overline{\tau}}'_\alpha$ is given by

$$(\overline{\overline{\tau}}'_\alpha)_{ij} - (\overline{\overline{\tau}}_\alpha)_{ij} = \rho_\alpha \left(w_{\alpha i} w_{\alpha j} - \frac{1}{3} w_\alpha^2 \delta_{ij} \right). \quad \text{(A22)}$$

Particle kinetic energy of thermal motion. The relationship between $\varepsilon_\alpha = \frac{m_\alpha \langle c_\alpha^2 \rangle}{2}$ and $\varepsilon'_a = \frac{m_\alpha \langle c_{\alpha 0}^2 \rangle'}{2}$

$$\varepsilon'_a = \varepsilon_\alpha + \frac{m_\alpha w_\alpha^2}{2}. \quad \text{(A23)}$$

$$\textit{Particle heat flux vector}: \quad \vec{q}_\alpha = \frac{1}{2}\rho_\alpha \langle c_\alpha^2 \vec{c}_\alpha \rangle, \quad \vec{q}'_a = \frac{1}{2}\rho_\alpha \langle c_{\alpha 0}^2 \vec{c}_{\alpha 0} \rangle.$$

After certain mathematical transformations:

$$c_{\alpha 0}^2 \vec{c}_{\alpha 0} = \left\langle (\vec{c}_\alpha + \vec{w}_\alpha)^2 (\vec{c}_\alpha + \vec{w}_\alpha) \right\rangle = \langle c_\alpha^2 \vec{c}_\alpha \rangle + 2\vec{w}_\alpha . \langle \vec{c}_\alpha \vec{c}_\alpha \rangle + \langle c_\alpha^2 \rangle \vec{w}_\alpha + w_\alpha^2 \vec{w}_\alpha.$$

Hence, having in mind that $\overline{\overline{P}}_\alpha = \rho_\alpha \langle \vec{c}_\alpha \vec{c}_\alpha \rangle$ and $n_\alpha \varepsilon_\alpha = \frac{1}{2}\rho_\alpha \langle c_\alpha^2 \rangle$, the relationship between $\vec{q}_\alpha$ and $\vec{q}_a{}'$ is

$$\vec{q}'_a = \vec{q}_\alpha + \vec{w}_\alpha . \overline{\overline{P}}_\alpha + n_\alpha \varepsilon_\alpha \vec{w}_\alpha + \frac{1}{2}\rho_\alpha w_\alpha^2 \vec{w}_\alpha. \quad \text{(A24)}$$

Total (plasma) kinetic pressure tensor $\overline{\overline{P}}$ is connected to the partial kinetic pressure tensor $\overline{\overline{P}}_\alpha$ by

$$\overline{\overline{P}} = \sum_\alpha \overline{\overline{P}}_\alpha + \sum_\alpha \rho_\alpha \vec{w}_\alpha \vec{w}_\alpha. \quad \text{(A25)}$$

Total scalar pressure p is connected to the partial scalar pressure p_α by

$$p = \sum_\alpha p_\alpha + \frac{1}{3}\sum_\alpha \rho_\alpha w_\alpha^2. \quad \text{(A26)}$$

The electric field seen by the charged particles when plasma moves with $\vec{u}$ is

$$\vec{E}' = \vec{E} + \vec{u} \times \vec{B}. \tag{A27}$$

The total electric current density or the charge flux, $\vec{J}$, and the conduction charge current density, $\vec{J}'$, are related by the convection current, $\rho\vec{u}$, where ρ is the total electric charge density

$$\vec{J} = \sum_{\alpha} n_{\alpha} Z_{\alpha} e \vec{u}_{\alpha} = \rho\vec{u} + \sum_{\alpha} n_{\alpha} Z_{\alpha} e \vec{w}_{\alpha} = \rho\vec{u} + \vec{J}'. \tag{A28}$$

The mobility of ions is low compared to the electron mobility and therefore, their contribution to the total current can be neglected. Hence, $\vec{J}$ is equivalent to the electron current density $\vec{J}_e = -n_e e \vec{u}_e$. Similarly, the total electric current density $\vec{J}'$ in the velocity representation relative to the plasma flow velocity $\vec{u}$, is $\vec{J}' = -n_e e \vec{w}_e$. The definitions of the total electric current density in both velocity representations, $\vec{J}$ and $\vec{J}'$, are equivalent when the plasma is neutral, i.e., $\rho = 0$.

In case of surface waves $\vec{J}$ is the electron current density, calculated by Equation (4).

Simplifications: The diffusion velocities $\vec{w}_{\alpha}$ are small compared to the thermal velocities $\vec{c}_{\alpha}$, and the quadratic terms in Equation (A19), (A20), and (A22–A26) can be neglected.[69] We receive the following relationships for the quantities in both velocity representations

$$\overline{\overline{P}}'_{\alpha} = \overline{\overline{P}}_{\alpha} = p_{\alpha}\overline{\overline{I}} + \overline{\overline{\tau}}_{\alpha}, \tag{A29a}$$

$$p'_{\alpha} = p_{\alpha}; \overline{\overline{\tau}}'_{\alpha} = \overline{\overline{\tau}}_{\alpha}, \tag{A29b}$$

$$\varepsilon'_{a} = \varepsilon_{\alpha}, \tag{A29c}$$

$$\vec{q}_a{}' = \vec{q}_{\alpha} + p_{\alpha}\vec{w}_{\alpha} + n_{\alpha}\varepsilon_{\alpha}\vec{w}_{\alpha} + \vec{w}_{\alpha}.\overline{\overline{\tau}}_{\alpha}, \tag{A29d}$$

$$\overline{\overline{P}} = \sum\nolimits_{\alpha} \overline{\overline{P}}_{\alpha}, \tag{A29e}$$

$$p = \sum\nolimits_{\alpha} p_{\alpha}, \tag{A29f}$$

$$\overline{\overline{\tau}} = \sum\nolimits_{\alpha} \overline{\overline{\tau}}_{\alpha}. \tag{A29g}$$

For isotropic distribution of the thermal velocity $\vec{c}_{\alpha}$, the plasma kinetic pressure tensor has the following form, taking into account Equation (A29e), (A29f), and (A29g):

$$\vec{\nabla}.\overline{\overline{P}} = \nabla p + \vec{\nabla}.\overline{\overline{\tau}}. \tag{A30}$$

The components of the plasma viscous stress tensor can be found from[70]

$$\tau_{ij} = -\left[\mu\left(\frac{\partial u_i}{\partial x_j} - \frac{\partial u_j}{\partial x_i}\right) + \mu_2 \delta_{ij}\left(\vec{\nabla}.\vec{u}\right)\right], \tag{A31}$$

where μ is the viscosity coefficient, and the coefficient μ_2 depends on the nature of the gas. For a mono-atomic gas $\mu_2 = -\frac{2}{3}\mu$.[70]

Finally, when the viscosity can be neglected the pressure tensor is connected to the partial scalar pressure by $\overline{\overline{P}}_{\alpha} = p_{\alpha}\overline{\overline{I}}$. Hence $\vec{w}_{\alpha}.\overline{\overline{P}}_{\alpha} = p_{\alpha}\vec{w}_{\alpha}$ and we receive for the particle heat flux vector

$$\vec{q}'_{a} = \vec{q}_{\alpha} + p_{\alpha}\vec{w}_{\alpha} + n_{\alpha}\varepsilon_{\alpha}\vec{w}_{\alpha}. \tag{A32}$$

Diffusion

Drift-Diffusion Approximation for Charged Particles

To analyze the transport of electrons we consider the specific density equation (A3) and specific momentum equation (A7a). To obtain the diffusion velocity we set the plasma flow velocity to 0 and neglect the time-variation.[70,71] Next, the electron diffusion velocity is much greater than the neutral particle diffusion velocity, and therefore the latter is neglected in the collision term. Hence, the momentum balance equation for the electrons becomes[70,71]

$$\frac{1}{n_e}\nabla(n_e k_B T_e) - e\vec{E} = -m_e \nu_m \vec{w}_e, \tag{A33}$$

which is the equation of motion of a single electron in a reference frame moving with the plasma or when the total plasma (gas) flow velocity is 0. From this equation the electron diffusion velocity in the so-called drift-diffusion approximation is obtained as[70,71]

$$\vec{w}_e = \frac{e}{m_e \nu_m}\vec{E} - \frac{k_B T_e}{m_e \nu_m}\frac{\nabla n_e}{n_e} - \frac{k_B T_e}{m_e \nu_m}\frac{\nabla T_e}{T_e}. \tag{A34}$$

The first term determines the directed (drift) velocity due to the acceleration in the external electric field, the second term describes the diffusion due to the density gradient, and the third term describes the (thermal) diffusion due to the temperature gradient. The proportionality factors are called electron mobility μ_e, and electron diffusion coefficient D_e

Plasma Process Polym **2017,** *14*, 1600185

$$\mu_e = \frac{e}{m_e \nu_m}; D_e = \frac{k_B T_e}{m_e \nu_m}. \quad \text{(A35)}$$

The relation between them is given by the Einstein relation: $\frac{D_e}{\mu_e} = \frac{k_B T_e}{e}$. In a similar way the ion diffusion velocity can be defined with corresponding properties: ion mobility μ_i, and ion diffusion coefficient D_i. Hence, the electron ($Z_e = -1$) and ion diffusion velocities are

$$\vec{w}_e = -\mu_e \vec{E} - \frac{1}{n_e} \nabla (D_e n_e), \quad \text{(A36)}$$

$$\vec{w}_i = Z_i \mu_i \vec{E} - \frac{1}{n_i} \nabla (D_i n_i). \quad \text{(A37)}$$

In plasma typically $\frac{\nabla T}{T} \ll \frac{\nabla n}{n}$ and the thermal diffusion can be neglected,[70] hence the second term is transformed to $-D_\alpha \frac{\nabla n_\alpha}{n_\alpha}$.

Ambipolar Diffusion Approximation for Charged Particles

The plasma is quasi-neutral in nature and only in a region adjacent to a solid surface the neutrality is not fulfilled. This region is referred to as a sheath. Its width is in the order of the Debye length λ_D, which is defined as the distance at which the plasma confines the electric field of a point charge.[71]

Let us assume that the quasi-neutrality in the plasma bulk is fulfilled at a given moment $n_e = n_i = n$. Since $m_e \ll m_i$, the electron mobility and diffusion coefficient are much greater than the ion mobility and diffusion coefficient, $\mu_e \gg \mu_i$ and $D_e \gg D_i$. Therefore, the electron flux exceeds the ion flux and the charge separation leads to the formation of an electric field, called ambipolar electric field, which speeds up the ions and retards the electrons. To maintain the quasi-neutrality, the changes in the electron and ion concentration in each volume element must be equal, that is, $\frac{\partial n_e}{\partial t} = \frac{\partial n_i}{\partial t}$.[70] Using Equation (A3) and the fact that an electron and ion appear or disappear simultaneously in a collision process, we find that independently of the plasma velocity $\vec{u}$, the following condition applies $\vec{\nabla}.(n_e \vec{w}_e) = \vec{\nabla}.(n_i \vec{w}_i)$.[70] This leads to the equality of the diffusion velocities of the electrons and ions. Hence, the ambipolar electric field in absence of an external electric field source can be found by applying Equation (A36) and (A37) for $Z_i = 1$. Using the obtained expression for the ambipolar electric field, the velocity of joint (ambipolar) motion of the charged particles is due to the density gradient[70]

$$\vec{w}_e = \vec{w}_i = \vec{w}_A = -D_A \frac{\nabla n}{n}, \quad \text{(A38)}$$

where the ambipolar diffusion coefficient D_A is:

$$D_A = \frac{\mu_i D_e + \mu_e D_i}{\mu_e + \mu_i} \approx \frac{\mu_i D_e}{\mu_e} + D_i = D_i \left(1 + \frac{T_e}{T_i}\right). \quad \text{(A39)}$$

The expression for D_A shows that the ambipolar diffusion coefficient is much smaller than the coefficient of free electron diffusion and greater than the free ion diffusion coefficient: $D_i < D_A \ll D_e$. Thus the ambipolar field reduces substantially the electron diffusion velocity.

The expression for the ambipolar diffusion coefficient is valid for a system with one dominant ionic species. For the Ar plasma under study, the density of the Ar^+ ion is 3–4 orders of magnitude larger than the density of the other positive, molecular ion $Ar_2{}^+$. Therefore, Equation (A39) can be applied in the developed QN model. In case of a complex mixture and electronegative plasmas, another method is needed.[83]

Diffusion of Neutral Particles, Fick's Model

The diffusion velocity of neutral particles can be found from Fick's law, which states that the diffusion flux $\vec{\Gamma}_{\alpha,dif} = n_\alpha \vec{w}_\alpha$ is proportional to the density gradient, that is,

$$n_\alpha \vec{w}_\alpha = -D_\alpha \nabla n_\alpha, \quad \text{(A41)}$$

where D_a is the diffusion coefficient of a species α. Fick's model for diffusion assumes that there is one dominant species and one type of particle moving through the background species. The atomic neutral gas in a weakly ionized plasma can be assumed to be a dominant species. In case of multiple types of particles Fick's model can be applied if all species have much lower number densities than the background gas. Indeed, the number densities of the electrons, ions and excited species are several orders of magnitude lower than the background neutral gas in the surface wave sustained plasma and in case of Ar there is one dominant species, which is the Ar atom in the ground state.

Heat Flux

The heat flux is found from the third moment of the BE. The general form can be found in[69] and the equation is difficult to solve without assumptions. For a stationary case, in absence of a magnetic field and for plasma flow velocity 0, the heat flow equation is simplified so that the heat flux is

proportional to the temperature gradient by a coefficient of proportionality called thermal conductivity coefficient λ_α[69,70]

$$\vec{q}_\alpha = -\lambda_\alpha \nabla(k_B T_\alpha). \quad \text{(A42)}$$

The thermal conductivity coefficient is defined as $\lambda_\alpha = \lambda_{T\alpha} n_\alpha$. The temperature conductivity coefficient $\lambda_{T\alpha}$ for the above stated assumptions is given by[69,70]

$$\lambda_{T\alpha} = \frac{5}{2}\frac{k_B T_\alpha}{m_e \nu_m} = \frac{5}{2} D_\alpha. \quad \text{(A43)}$$

Hence, the temperature conductivity coefficient is comparable to the diffusion coefficient.

When the plasma flow is not 0, the heat flux vector in a laboratory reference frame is given by Equation (A32).

Received: August 31, 2016; Revised: October 14, 2016; Accepted: October 20, 2016; DOI: 10.1002/ppap.201600185

Keywords: computer modeling; microwave discharges; non-thermal plasma; optical emission spectroscopy (OES)

[1] M. Moisan, A. Shivarova, A. W. Trivelpiece, *Plasma Phys*. **1982**, *24*, 1331.
[2] M. Moisan, J. Pelletier (Eds.), Microwave Excited Plasmas, Elsevier, Amsterdam, the Netherlands **1992**.
[3] H. Schlüter, A. Shivarova, *Phys. Rep*. **2007**, *443*, 121.
[4] Yu. A. Lebedev, *J. Phys.: Conf. Ser*. **2010**, *257*, 012016.
[5] F. Normand, J. Marec, Ph. Leprince, A. Granier, *Mater. Sci. Eng. A* **1991**, *139*, 103.
[6] R. Foest, E. Kindel, A. Ohl, M. Stieber, K.-D. Weltmann, *Plasma Phys. Control. Fusion* **2005**, *47*, B525.
[7] D. Vinga Szabó, S. Schlabach, *Inorganics* **2014**, *2*, 468.
[8] L. Zajíčková, O. Jašek, P. Synek, A. Obrusník, V. Kudrle, *Conference Proceedings MD9 "Microwave Discharges: Fundamentals and Applications"*. UCOPress, Cordoba **2015**.
[9] A. Dias, N. Bundaleski, E. Tatarova, F. M. Dias, M. Abrashev, U. Cvelbar, O. M. N. D. Teodoro, J. Henriques, *J. Phys. D: Appl. Phys*. **2016**, *49*, 055307.
[10] H. Kokura, K. Nakamura, I. Ghanashev, H. Sugai, *Jpn. J. Appl. Phys*. **1999**, *38*, 5262.
[11] M. Moisan, J. Barbeau, M.-C. Crevier, J. Pelletier, N. Philip, B. Saoudi, *Pure Appl. Chem*. **2002**, *74*, 349.
[12] N. Philip, B. Saoudi, M. Moisan, J. Barbeau, J. Pelletier, *IEEE Trans. Plasma Sci*. **2002**, *30*, 1429.
[13] J Ehlbeck, A Ohl, M Maaß, U Krohmann, T Neumann, *Surf. Coat. Technol*. **2003**, *174–175*, 493.
[14] G. Fridman, G. Friedman, A. Gutsol, A. B. Shekhter, V. N. Vasilets, A. Fridman, *Plasma Process. Polym* **2008**, *5*, 503.
[15] J. Heinlin, G. Morfill, M. Landthaler, W. Stolz, G. Isbary, J. L. Zimmermann, T. Shimizu, S. Karrer, *J. Dtsch. Dermatol. Ges*. **2010**, *8*, 968.
[16] M. Baeva, M. Andrasch, J. Ehlbeck, D. Loffhagen, K.-D. Weltmann, *J. Appl. Phys*. **2014**, *115*, 143301.
[17] S. Schermer, N. H. Bings, A. M. Bilgiç, R. Stonies, E. Voges, J. A. C. Broekaert, *Spectrochim. Acta B* **2003**, *58*, 1585.
[18] A. R. Hoskinson, J. Hopwood, N. W. Bostrom, J. A. Crank, C. Harrison, *J. Anal. At. Spectrom*. **2011**, *26*, 1258.
[19] Y. Kabouzi, M. Moisan, J. C. Rostaing, C. Trassy, D. Guérin, D. Kéroack, Z. Zakrzewski, *J. Appl. Phys*. **2003**, *93*, 9483.
[20] Welzel, S.; Bongers, W. A.; Graswinckel, M. F.; van de Sanden, M. C. M., *PS Gaseous Electronics Conference* **2014**, abstract #SF2.006 "CO_2 dissociation in vortex-stabilized microwave plasmas".
[21] G. Chen, V. Georgieva, T. Godfroid, R. Snyders, M.-P. Delplancke-Ogletree, *Appl. Catal. B-Environ*. **2016**, *190*, 115.
[22] A. W. Trivelpiece, R. W. Gould, *J. Appl. Phys*. **1959**, *30*, 1784.
[23] M. Moisan, C. Beaudry, P. Leprince, *Phys. Lett*. **1974**, *50A*, 125.
[24] Z. Zakrzewski, *J. Phys. D: Appl. Phys*. **1983**, *16*, 171.
[25] C. M. Ferreira, *J. Phys. D: Appl. Phys*. **1983**, *16*, 1673.
[26] C. Boisse-Laporte, A. Graniert, E. Dervisevic, P. Leprince, J. Marec, *J. Phys. D: Appl. Phys*. **1987**, *20*, 197.
[27] C. M. Ferreira, M. Moisan, *Phys. Scr*. **1988**, *38*, 382.
[28] Yu. M. Aliev, I. Ganashev, H. Schlüter, A. Shivarova, M. Zethoff, *Plasma Sources Sci. Technol*. **1994**, *3*, 216.
[29] Yu. M. Aliev, H. Schlüter, A. Shivarova, *Guided-Wave-Produced Plasmas*. Springer-Verlag, Berlin Heidelberg, Germany **2000**.
[30] E. Mateev, I. Zhelyazkov, V. Atanassov, *J. Appl. Phys*. **1983**, *54*, 3049.
[31] I. Zhelyazkov, E. Benova, *J. Appl. Phys*. **1989**, *66*, 1641.
[32] E. Benova, I. Zhelyazkov, *Phys. Scr*. **1991**, *43*, 68.
[33] C. M. Ferreira, *J. Phys. D: Appl. Phys*. **1989**, *22*, 705.
[34] U. Kortshagen, H. Schlüter, A. Shivarova, *J. Phys. D: Appl. Phys*. **1991**, *24*, 1571.
[35] L. L. Alves, G. Gousset, C. M. Ferreira, *J. Phys. D: Appl. Phys*. **1992**, *25*, 1713.
[36] Ts. Petrova, E. Benova, G. Petrov, I. Zhelyazkov, *Phys. Rev. E* **1999**, *60*, 875.
[37] J. Henriques, E. Tatarova, F. M. Dias, C. M. Ferreira, *J. Appl. Phys*. **2001**, *90*, 4921.
[38] L. L. Alves, S. Letout, C. Boisse-Laporte, *Phys. Rev. E* **2009**, *79*, 016403.
[39] G. M. Janssen, *PhD Thesis*, Eindhoven University of Technology, the Netherlands, October, **2000**.
[40] Y. Kabouzi, D. B. Graves, E. Castaños-Martínez, M. Moisan, *Phys. Rev. E* **2007**, *75*, 016402.
[41] M. Jimenez-Diaz, E. A. D. Carbone, J. van Dijk, J. J. A. M. van der Mullen, *J. Phys. D: Appl. Phys*. **2012**, *45*, 335204.
[42] S. Rahimi, M. Jimenez-Diaz, S. Hubner, E. H. Kemaneci, J. J. A. M. van der Mullen, J. van Dijk, *J. Phys. D: Appl. Phys*. **2014**, *47*, 125204.
[43] Z. Zakrzewski, M. Moisan, V. M. M. Glaude, C. Beaudry, P. Leprince, *Plasma Phys*. **1977**, *19*, 77.
[44] J. Margot-Chaker, M. Moisan, M. Chaker, V. M. M. Glaude, P. Lauque, J. Paraszczak, G. Sauvé, *J. Appl. Phys*. **1989**, *66*, 4134.
[45] M. Moisan, Z. Zakrzewski, *J. Phys. D: Appl. Phys*. **1991**, *24*, 1025.
[46] E Bloyet, P Leprince, M. Llamas Blasco, J Marec, *Phys. Lett. A* **1981**, *83*, 391.
[47] T. Godfroid, J. P. Dauchot, M. Hecq, *Surf. Coat. Technol*. **2003**, *174–175*, 1276.
[48] M. C. Garćıa, A. Rodero, A. Sola, A. Gamero, *Spectrochim. Acta Part B* **2000**, *55*, 1733.
[49] C. Lao, A. Gamero, A. Sola, Ts. Petrova, E. Benova, G. M. Petrov, I. Zhelyazkov, *J. Appl. Phys* **2000**, *87*, 7652.
[50] J. M. Palomares, E. Iordanova, E. M. van Veldhuizen, L. Baede, A. Gamero, A. Sola, J. J. A. M. van der Mullen, *Spectrochim. Acta Part B* **2010**, *65*, 225.

[51] N. Britun, T. Godfroid, R. Snyders, *Plasma Sources Sci. Technol.* **2012**, *21*, 035007.
[52] S. Hübner, N. Sadeghi, E. A. D. Carbone, J. J. A. M. van der Mullen, *J. Appl. Phys* **2013**, *113*, 143306.
[53] L. D. Landau, E. M. Lifshiftz, *Electrodynamics of Continuous Media*. Pergamon Press, Oxford **1960**.
[54] G. J. M. Hagelaar, K. Hassouni, A. Gicquel, *J. Appl. Phys*. **2004**, *96*, 1819.
[55] A. Sola, A. Gamero, J. Cotrino, V. Colomer, *J. Phys. D: Appl. Phys*. **1988**, *21*, 1112.
[56] J. Cotrino, A. Gamero, A. Sola, V. Colomer, *J. Phys. D: Appl. Phys*. **1988**, *21*, 1377.
[57] St. Kolev, A. Bogaerts, *Plasma Sources Sci. Technol*. **2015**, *24*, 015025.
[58] J. B. Boffard, R. O. Jung, C. C. Lin, A. E. Wendt, *Plasma Sources Sci. Technol*. **2010**, *19*, 065001.
[59] T. Silva, N. Britun, T. Godfroid, J. van der Mullen, R. Snyders, *J. Appl. Phys*. **2016**, *119*, 173302.
[60] N. Britun, M. Gaillard, S. Oh, J. Han, *J. Phys. D: Appl. Phys*. **2007**, *40*, 5098.
[61] G. M. Janssen, J. van Dijk, D. A. Benoy, M. A. Tas, K. T. A. L. Burm, W. J. Goedheer, J. A. M. van der Mullen, D. C. Schram, *Plasma Sources Sci. Technol*. **1999**, *8*, 1.
[62] J. van Dijk, K. Peerenboom, M. Jimenez, D. Mihailova, J. van der Mullen, *J. Phys. D: Appl. Phys*. **2009**, *42*, 194012.
[63] The Plasimo Team, Homepage, https://plasimo.phys.tue.nl/ (accesses November, 2016).
[64] COMSOL Inc, Homepage, https://www.comsol.com (accessed November, 2016).
[65] D. A. Benoy, *PhD Thesis*, Eindhoven University of Technology, the Netherlands, April **1993**.
[66] M. A. Liebermann, A. J. Lichtenberg, *Principles of Plasma Discharges and Materials processing*. Wiley, New York, USA **1994**.
[67] G. J. M. Hagelaar, L. C. Pitchford, *Plasma Sources Sci. Technol.* **2005**, *14*, 722.
[68] M. Jimenez-Diaz, *PhD Thesis*, Eindhoven University of Technology, the Netherlands, June **2011**.
[69] J. A. Bittencourt, *Fundamentals of Plasma Physics*. Springer-Verlag, New York, USA **2004**.
[70] V. E. Golant, A. P. Zhilinskii, I. E. Sakharov, *Fundamentals of Plasma Physics*. Wiley, New York, USA **1980**.
[71] M. Mitchner, C. H. Kruger, *Partially Ionized Gases*. Wiley, New York, USA **1973**.
[72] E. W. McDaniel, E. A. Mason, *The Mobility and Diffusion of Ions in Gases*. Wiley, Hoboken, NJ, USA **1973**.
[73] C. M. Ferreira, J. Loureiro, A. Ricard, *J. Appl. Phys*. **1985**, *57*, 82.
[74] R. S. Devoto, *Phys. Fluids* **1967**, *10*, 2105.
[75] J. O. Hirschfelder, C. F. Curtiss, R. B. Bird, *Molecular Theory of Gases and Liquids* Wiley, New York, USA **1954**, Ch. 7 and 8.
[76] J. Jolly, M. Touzeau, *J. Quant. Spectrosc. Radiat. Transfer*. **1975**, *15*, 863.
[77] T. Fujimoto, *Plasma Spectroscopy* Oxford University Press Inc., New York, USA **2004**.
[78] M. Schulze, A. Yanguas-Gil, A. Keudell, P. Awakowicz, *J. Phys. D: Appl. Phys*. **2008**, *41*, 065206.
[79] V. Sushkov, H. Do, R. Hippler, *Contrib. Plasma Phys*. **2013**, *53*, 549.
[80] A. Phelps, *Phys. Rev*. **1958**, *110*, 1362.
[81] S. G. Rabinovich, *Evaluating Measurement Accuracy: A practical Approach* Springer-Verlag, New York, USA **2010**, p. 148.
[82] Y. Li, M. H. Gordon, L. A. Roe, K. Hassouni, T. Grotjohn, *J. Appl. Phys*. **2003**, *94*, 85.
[83] A. Hartgers, G. M. Janssen, J. J. A. M. van der Mullen, *J. Phys. D: Appl. Phys*. **2003**, *36*, 114.